A metric-based mesh adaptation for hybrid RANS/LES flow calculations

September 2024

Bastien Sauvage

Université Côte d'Azur, INRIA,

2004 Route des lucioles, F-06902 Sophia-Antipolis, bastien.sauvage@inria.fr

Bruno Koobus

IMAG, université de Montpellier

Montpellier

Frédéric Alauzet

Université Paris-Saclay- INRIA, 1, rue Honoré d'Estienne d'Orves F-91126

Palaiseau

Alain Dervieux

Société technologique LEMMA, 2000 route des Lucioles, Sophia-Antipolis, France,

and Université Côte d'Azur, INRIA, 2004 Route des lucioles,

F-06902 Sophia-Antipolis

Abstract:

We present a mesh adaptation method for CFD calculations of compressible flows with hybrid RANS/LES turbulence models. The anisotropic mesh representation is based on the continuous mesh approach using metrics. Two adaptation criteria are combined, one for controling the numerical error in solving the URANS equations, and one for controlling the LES error model. The second criterion is based the Toosi-Larsson formulation derived from the Germano analysis. Numerical examples of mesh adaptive LES calculations of flows around blunt bodies are reported and analysed.

Keywords: Compressible flow, Hyperbolic, Euler flow, Finite volume, Error estimation, Mesh adaptation.

Contents

List of Figures

List of Tables

1 Introduction

Large Eddy Simulations (LES) and hybrid flow calculations for turbulent flow are today still very computer consuming CFD activities. More importantly, the user has difficuties in deciding if the mesh used produces the expected accuracy. Upgrading mesh adaptation methods to a better treatment of LES/hybrid flows is then an important issue. Unlike a statistical turbulence model, which tends to neglect fluctuations by applying a statistical average which in most cases damps all these fluctuations, LES can be interpreted as damping only a part of unsteady turbulent structures, typically structures with a scale smaller than a prescribed filter size. The smallest structures being the most difficult to resolve, LES consumes much less computational resources than a Direct Numerical Simulation which computes all turbulence structures. LES modelling therefore relies on two steps:
(i)- defining the neglected scales as those which are smaller than a filter width Δ_f and adding a model of the action of neglected scales on the non-neglected ones. This defines a continuous model parameterized by the filter width Δ_f,
(ii)- using, in order to approximate the continuous model built in (i), a mesh-based approximation with local mesh size Δ_g, typically:

$$\Delta_g = (\xi\eta\zeta)^{\frac{1}{3}} \tag{1}$$

(expressed directly in terms of the local mesh sizes (ξ, η, ζ) measured in three orthogonal directions). While, by construction, Δ_f should be larger than Δ_g, in order to approximate accurately the non-neglected scales, the research of the lowest computational cost motivates the practitioner to set

$$\Delta_f = \Delta_g,$$

with the consequence that the smallest unfiltered scales are the smallest scales computed on the grid and are then very poorly approximated, whatever be the accuracy of the numerical scheme.

When using a second-order accurate approximation, an important disadvantage comes from the fact that many LES models of Smagorinsky type are similar to second-order accurate truncation terms, in such a way that approximation errors are of same order as the filter model. According to an analysis of Ghosal [15] and to the outputs of many numerical computations, see e.g. [18], using a second-order accurate approximation may result in errors larger than the effect of LES modelling. It remains that second-order accurate approximations are often used and very useful for computing

LES flows in engineering. A good practise for increasing the confidence in second-order accurate LES computations is to compare (a) the LES-based computations with (b) their no-model counterpart of order two, see e.g. [20].

Let assume that an approximation with a truncation error of order α is used. An important issue is the fact that the convergence at truncation order is subject to the condition of using a sufficiently refined mesh: the mesh should be in any point sufficiently fine for capturing the smallest local detail of the flow computed, in order to obtain second-order or higher order convergence. This desserves some comments.

- Already in steady CFD, the convergence at truncation order is difficult to attain. A very efficient tool for obtaining this convergence is the convergent mesh adaptive double loop as described in [1, 11]. The inner loop is an anisotropic metric-based fixed-point *adaptation* working with a fixed number of unknowns. The outer loop is an anisotropic metric-based *enrichment* increasing progressively the total number of unknowns and controlling the actual convergence to the continuous solution. Thanks to this double loop, steady second-order RANS calculations are reaching a higher level of accuracy and fiability.
- As concerns unsteady RANS, mesh convergence with a double mesh adaptive loop is more difficult to apply, but effective in many cases. See for examples [4], [24], [22].
- As concerns mesh convergence with LES, it is a much more difficult issue. The brute-force strategy which increases simply the number of nodes generally may not succeed for the following reason. Refining the mesh diminishes the subgrid-scale (SGS) term and introduces the arising of smaller and smaller new unstable scales in the solution which therefore cannot be accurately approximated until the process simply solves the corresponding DNS flow. Therefore, in contrast to laminar and RANS modeling, mesh adaptation for LES and hybrid models cannot have as goal the faster/fastest convergence to a continuous field, except the generally not offerdable exact solution of Navier-Stokes.

The designing of a mesh adaptation criterion for LES is an important and difficult issue, addressed by many publications, among which we have selected the following typical ones.

In [5], the approach is a numerical one, related to truncation error. The error estimator identifies the regions lacking in accuracy, improving their resolution by either decreasing the size of the element or increasing the polynomial degree which approximates locally the solution. A smoothness indicator guides the *hp*-decision, leading to *p*-enrichment for smooth regions and h-refinement for non-smooth regions.

The work in [17] compares three indicators. The first indicator is based on the unsteady residual. The second indicator is based on a local smoothness indicator. The third indicator is based on an estimate for small scale turbulent kinetic energy. Comparisons with DNS tend to show that the first indicator is the best.

Similarly, in [16] several indicators more or less related to discretization and modeling error are compared with a wall jet as main test case.

In [13], a field-inversion machine-learning (FIML) framework is introduced. It only requires unsteady primal solutions. Two error estimates are compared in this work, a time-averaged unsteady residual weighted by a time-averaged adjoint, and an augmented-system residual weighted by the augmented-system adjoint.

In [21] the approach relies on a Discontinuous Galerkin (DG) high-order approximation. It does not really propose a mesh adaptation, but defines the ideal DG-LES solution as the result of the application of two successive filtering operations. A first convolution filter is applied to the DNS data which filters out frequencies beyond the LES grid cut-off. Next, a L^2-projection of this filtered field is performed on the *hp*-discretization space.

The physical approach is better addressed in [8]: arguments are based on the ratio of subgrid to viscous dissipation or viscosity. They are meaningful only in the buffer layer of wall-bounded turbulence while LES should be applicable to free shear flows at any Reynolds number.

In contrast to these contributions, we look for a satisfactory measure of the actual modelling error induced by LES. We discuss now an interesting analysis of this error. We have observed that, in most models, the local filter size introduced in practical LES models is generally taken identical to the local mesh size. Therefore informations concerning the improvement of the filter size can be useful for the improvement of mesh size. This is why we discuss now the work of Germano and co-workers [14] which have proposed a measure of the modelling error and a method for reducing it by adapting the filter size. We use the notations of [29] where this method is also explained. If a filter $W \mapsto \bar{W}$ of size $\bar{\Delta}$ is applied to the continuous (incompressible)

Navier-Stokes equations for the exact field $(\mathcal{U}, \mathcal{P})$:

$$\mathcal{N}(\mathcal{U}) = \frac{\partial \mathcal{U}_i}{\partial t} + \frac{\partial \mathcal{U}_i \mathcal{U}_j}{\partial x_j} + \frac{1}{\rho}\frac{\partial \mathcal{P}}{\partial x_j} - \nu \frac{\partial^2 \mathcal{U}_i}{\partial x_j \partial x_j} = 0 \tag{2}$$

then the coarse-grained representation $(\overline{\mathcal{U}}, \overline{\mathcal{P}})$ of the exact field satisfies:

$$\begin{aligned} \mathcal{N}^{exact}_{\bar{\Delta}}(\overline{\mathcal{U}}) &= \frac{\partial \overline{\mathcal{U}}_i}{\partial t} + \frac{\partial \overline{\mathcal{U}}_i \overline{\mathcal{U}}_j}{\partial x_j} + \frac{1}{\rho}\frac{\partial \overline{\mathcal{P}}}{\partial x_j} - \nu \frac{\partial^2 \overline{\mathcal{U}}_i}{\partial x_j \partial x_j} + \frac{\partial \tau^{exact}_{ij,\bar{\Delta}}}{\partial x_j} = 0 \\ \text{with} \quad \tau^{exact}_{ij,\bar{\Delta}} &= \overline{\mathcal{U}_i \mathcal{U}_j} - \overline{\mathcal{U}}_i \overline{\mathcal{U}}_j . \end{aligned} \tag{3}$$

The basic idea of Germano's analysis is to introduce a second filter, not used directly in the model, the *filter test* with a size $\hat{\Delta} > \bar{\Delta}$ slightly larger than the LES filter. If we apply successively filter $\bar{\cdot}$ and test filter $\hat{\cdot}$ to $\mathcal{U}$, denoting $\tau^{exact}_{ij,\hat{\bar{\Delta}}} = \widehat{\overline{\mathcal{U}_i \mathcal{U}_j}} - \widehat{\overline{\mathcal{U}}}_i \widehat{\overline{\mathcal{U}}}_j$, we have

$$\mathcal{N}^{exact}_{\hat{\bar{\Delta}}}(\widehat{\overline{\mathcal{U}}}) = \frac{\partial \widehat{\overline{\mathcal{U}}}_i}{\partial t} + \frac{\partial \widehat{\overline{\mathcal{U}}}_i \widehat{\overline{\mathcal{U}}}_j}{\partial x_j} + \frac{1}{\rho}\frac{\partial \widehat{\overline{\mathcal{P}}}}{\partial x_j} - \nu \frac{\partial^2 \widehat{\overline{\mathcal{U}}}_i}{\partial x_j \partial x_j} + \frac{\partial \tau^{exact}_{ij,\hat{\bar{\Delta}}}}{\partial x_j} = 0,$$

while applying $\hat{\cdot}$ to $\mathcal{N}^{exact}_{\bar{\Delta}}(\overline{\mathcal{U}})$ gives:

$$\widehat{\mathcal{N}^{exact}_{\bar{\Delta}}(\overline{\mathcal{U}})} = \frac{\partial \widehat{\overline{\mathcal{U}}}_i}{\partial t} + \frac{\partial \widehat{\overline{\mathcal{U}}_i \overline{\mathcal{U}}_j}}{\partial x_j} + \frac{1}{\rho}\frac{\partial \widehat{\overline{\mathcal{P}}}}{\partial x_j} - \nu \frac{\partial^2 \widehat{\overline{\mathcal{U}}}_i}{\partial x_j \partial x_j} + \frac{\partial \widehat{\tau^{exact}_{ij,\bar{\Delta}}}}{\partial x_j} = 0$$

then

$$\mathcal{N}^{exact}_{\hat{\bar{\Delta}}}(\widehat{\overline{\mathcal{U}}}) - \widehat{\mathcal{N}^{exact}_{\bar{\Delta}}(\overline{\mathcal{U}})} = \frac{\partial}{\partial x_j}\left(\widehat{-\tau^{exact}_{ij,\bar{\Delta}}} + \tau^{exact}_{ij,\hat{\bar{\Delta}}} \; - \; \widehat{\overline{\mathcal{U}}_i \overline{\mathcal{U}}_j} + \widehat{\overline{\mathcal{U}}}_i \widehat{\overline{\mathcal{U}}}_j \right) \tag{4}$$

Statement (4) can be interpreted as an approximate equation for the filtering error $\widehat{\overline{\mathcal{U}}} - \overline{\mathcal{U}}$. In [14] the *Germano identity* is shown:

$$\widehat{-\tau^{exact}_{ij,\bar{\Delta}}} + \tau^{exact}_{ij,\hat{\bar{\Delta}}} \; - \; \widehat{\overline{\mathcal{U}}_i \overline{\mathcal{U}}_j} + \widehat{\overline{\mathcal{U}}}_i \widehat{\overline{\mathcal{U}}}_j = 0.$$

and the RHS of (4) is zero. The Germano identity is true for continuous solutions of the exact Navier-Stokes system but will not apply if the exact

Navier-Stokes system is replaced by a continuous formulation of a LES model *with one filter* with $\bar{u}$ as solution:

$$\mathcal{N}^{model}_{\bar\Delta}(\overline{u}) = \frac{\partial \overline{u}_i}{\partial t} + \frac{\partial \overline{u}_i \overline{u}_j}{\partial x_j} + \frac{1}{\rho}\frac{\partial \overline{p}}{\partial x_j} - \nu \frac{\partial^2 \overline{u}_i}{\partial x_j \partial x_j} + \frac{\partial \tau^{model}_{ij,\bar\Delta}(\overline{u})}{\partial x_j} = 0 \qquad (5)$$

To fix the ideas, for the Smagorinsky model (incompressible case), it writes:

$$\begin{array}{l} \tau^{model}_{ij,\bar\Delta}(\overline{u}) = -(C_s\bar\Delta)^2|S|P_{ij} \\ S_{ij} = \frac{1}{2}(\frac{\partial \bar{u}_i}{\partial x_j} + \frac{\partial \bar{u}_j}{\partial x_i}) \\ P_{ij} = 2S_{ij} - \frac{2}{3}S_{kk}\delta_{ij} \end{array} \qquad (6)$$

C_s being the Smagorinsky constant (typically, $C_s = 0.1$).

A second formulation is the formulation *with both filters* with $\widehat{\overline{v}}$ as solution:

$$\mathcal{N}^{model}_{\hat{\bar\Delta}}(\widehat{\overline{v}}) = \frac{\partial \widehat{\overline{v}}_i}{\partial t} + \frac{\partial \widehat{\overline{v}}_i \widehat{\overline{v}}_j}{\partial x_j} + \frac{1}{\rho}\frac{\partial \widehat{\overline{p}}}{\partial x_j} - \nu \frac{\partial^2 \widehat{\overline{v}}_i}{\partial x_j \partial x_j} + \frac{\partial \tau^{model}_{ij,\hat{\bar\Delta}}(\widehat{\overline{v}})}{\partial x_j} = 0. \qquad (7)$$

which implies that:

$$\widehat{\mathcal{N}^{model}_{\bar\Delta}(\overline{u})} - \mathcal{N}^{model}_{\hat{\bar\Delta}}(\widehat{\overline{u}}) = \frac{\partial}{\partial x_j}\Big(\widehat{\tau^{model}_{ij,\bar\Delta}(\overline{u})} \; - \; \tau^{model}_{ij,\hat{\bar\Delta}}(\widehat{\overline{u}}) \; + \; \widehat{\overline{u}_i\overline{u}_j} - \widehat{\overline{u}}_i\widehat{\overline{u}}_j\Big) \qquad (8)$$

which RHS is in general not zero. Although discarding the divergence $\frac{\partial}{\partial x_j}$, the Germano identity error

$$\mathcal{G}_{ij} \; = \; \widehat{\tau^{model}_{ij,\bar\Delta}(\overline{u})} \; - \; \tau^{model}_{ij,\hat{\bar\Delta}}(\widehat{\overline{u}}) \; + \; \widehat{\overline{u}_i\overline{u}_j} - \widehat{\overline{u}}_i\widehat{\overline{u}}_j$$

is a (tensorial) measure of the error between the (non-discretized) Navier Stokes flow field and the (non-discretized) LES flow field. Therefore, the Dynamic Germano-Piomelli procedure, by minimizing in some sense the Germano identity error, allows to find either the *optimal coefficient* C_s, or the *optimal product* $C_s\bar\Delta$ (both used in (6)). In the Dynamic Germano-Piomelli practice, $\bar{u}$ is not known and is replaced by its discrete analog $\bar{u}_h$ computed on a given mesh, the filter size $\bar\Delta$ is generally chosen as the local mesh size, the filter test is chosen as $\kappa_{\bar\Delta}\bar\Delta$, where $\kappa_{\bar\Delta}$ is frozen to the value 2. Then a new product $(C_s\bar\Delta)_{optimum}$ which reduces the RHS of (8) is computed. This is usually interpreted as giving a new local value $(C_s)_{optimum} = (C_s\bar\Delta)_{optimum}/\bar\Delta$.

Assuming now that we do not want to change C_s, the same computation proposes a new value for $\bar{\Delta}$:

$$(\bar{\Delta})_{optimum} = (C_s\bar{\Delta})_{optimum}/C_s$$

which seems to give informations concerning the filter, and then concerning the mesh to use.

The dynamic Germano analysis has inspired Toosi and Larsson [28] in proposing a method for adapting the mesh to a LES formulation. Toosi and Larsson identify *the source of LES-modelling error* as the residual of the governing LES equation applied to the coarse-grained exact Navier-Stokes solution. For a filter level $\bar{\Delta}$:

$$\mathcal{R}_{i,\bar{\Delta}} \equiv \mathcal{N}^{model}_{\bar{\Delta}}(\overline{\mathcal{U}}) = \frac{\partial \overline{\mathcal{U}}_i}{\partial t} + \frac{\partial \overline{\mathcal{U}}_i\overline{\mathcal{U}}_j}{\partial x_j} + \frac{1}{\rho}\frac{\partial \overline{\mathcal{P}}}{\partial x_j} - \nu\frac{\partial^2 \overline{\mathcal{U}}_i}{\partial x_j \partial x_j} + \frac{\partial \tau^{model}_{ij,\bar{\Delta}}(\overline{\mathcal{U}})}{\partial x_j}$$

and, using (3), we get

$$\mathcal{R}_{i,\bar{\Delta}} = \frac{\partial}{\partial x_j}\big[\tau^{model}_{ij,\bar{\Delta}}(\overline{\mathcal{U}}) - \tau^{exact}_{ij,\bar{\Delta}}\big].$$

Similarly, for filter test $\widehat{\bar{\Delta}}$:

$$\mathcal{R}_{i,\widehat{\bar{\Delta}}} \equiv \mathcal{N}^{model}_{\widehat{\bar{\Delta}}}(\widehat{\overline{\mathcal{U}}}) = \frac{\partial}{\partial x_j}\big[\tau^{model}_{ij,\widehat{\bar{\Delta}}}(\widehat{\overline{\mathcal{U}}}) - \tau^{exact}_{ij,\widehat{\bar{\Delta}}}\big]. \tag{9}$$

The residual $\mathcal{R}_{i,\widehat{\bar{\Delta}}}$ is chosen as the *error source of the LES modelling* but is expressed in terms of the unknown exact solution $\mathcal{U}$. In order to use it in practice, we need to replace $\mathcal{U}$ by an approximate evaluation of it. The *fundamental approximation* done by Toosi and Larsson is replacing in $\mathcal{N}^{model}_{\widehat{\bar{\Delta}}}$ the coarse-grained exact Navier-Stokes solution $\widehat{\overline{\mathcal{U}}}$ by the LES one $\widehat{\overline{u}}$:

$$\mathcal{R}_{i,\widehat{\bar{\Delta}}} \equiv \mathcal{N}^{model}_{\widehat{\bar{\Delta}}}(\widehat{\overline{\mathcal{U}}}) \approx \mathcal{N}^{model}_{\widehat{\bar{\Delta}}}(\widehat{\overline{u}}) \tag{10}$$

thus:

$$\mathcal{R}_{i,\widehat{\bar{\Delta}}} \approx \frac{\partial \widehat{\overline{u}}_i}{\partial t} + \frac{\partial \widehat{\overline{u}}_i\widehat{\overline{u}}_j}{\partial x_j} + \frac{1}{\rho}\frac{\partial \widehat{\overline{p}}}{\partial x_j} - \nu\frac{\partial^2 \widehat{\overline{u}}_i}{\partial x_j \partial x_j} + \frac{\partial \tau^{model}_{ij,\widehat{\bar{\Delta}}}(\widehat{\overline{u}})}{\partial x_j}$$

which is transformed applying the test-filtering to (5):

$$\frac{\partial \hat{\overline{u}}_i}{\partial t} + \frac{\partial \widehat{\overline{u}_i \overline{u}_j}}{\partial x_j} + \frac{1}{\rho}\frac{\partial \hat{\overline{p}}}{\partial x_j} - \nu \frac{\partial^2 \hat{\overline{u}}_i}{\partial x_j \partial x_j} + \frac{\partial \widehat{\tau^{model}_{ij,\bar{\Delta}}(\overline{u})}}{\partial x_j} = 0,$$

and then substracting the result from (10). This gives:

$$\mathcal{R}_{i,\hat{\bar{\Delta}}} \approx \mathcal{F}_{i,\hat{\bar{\Delta}}} = \frac{\partial}{\partial x}\Big[\tau^{model}_{ij,\hat{\bar{\Delta}}}(\hat{\overline{u}}) \ - \ \widehat{\tau^{model}_{ij,\bar{\Delta}}(\overline{u})} - \widehat{\overline{u}_i \overline{u}_j} + \hat{\overline{u}}_i \hat{\overline{u}}_j\Big]. \tag{11}$$

In order to minimize the RHS of (11), the authors consider a directional test filter $\hat{\cdot}^{\mathbf{n}_x}$ of size $\bar{\Delta}_{\mathbf{n}_x}$, in direction $\mathbf{n}_x$:

$$\hat{\bar{\phi}}^{(\mathbf{n}_x)} \approx \left(I + \frac{\bar{\Delta}^2_{\mathbf{n}_x}}{4}\mathbf{n}_x^T \nabla \nabla^T \mathbf{n}_x\right) \bar{\phi}. \tag{12}$$

Applying the directional test filter to equation (5) gives the following evolution equation for the filtered instantaneous fields at the filter test level:

$$\frac{\partial \hat{\overline{u}}_i^{(\mathbf{n}_x)}}{\partial t} + \frac{\partial \widehat{\overline{u}_i \overline{u}_j}^{(\mathbf{n}_x)}}{\partial x_j} + \frac{1}{\rho}\frac{\partial \hat{\overline{p}}^{(\mathbf{n}_x)}}{\partial x_j} - \nu \frac{\partial^2 \hat{\overline{u}}_i^{(\mathbf{n}_x)}}{\partial x_j \partial x_j} + \frac{\partial \widehat{\tau^{model}_{ij}(\overline{u})}^{(\mathbf{n}_x)}}{\partial x_j} = 0. \tag{13}$$

Following the above calculation in this directional context, the following source term analog to (11) is obtained:

$$\hat{\bar{\mathcal{F}}}_i^{(\mathbf{n}_x)}(\mathbf{x}) = \frac{\partial}{\partial x_j}\left(\tau^{model}_{ij}(\hat{\overline{u}}^{(\mathbf{n}_x)}) - \widehat{\tau^{model}_{ij}(\overline{u})}^{(\mathbf{n}_x)} - \widehat{\overline{u}_i \overline{u}_j}^{(\mathbf{n}_x)} + \hat{\overline{u}}_i^{(\mathbf{n}_x)} \hat{\overline{u}}_j^{(\mathbf{n}_x)}\right) \tag{14}$$

and the Toosi-Larsson method proposes to minimize with respect to $\bar{\Delta}_{\mathbf{n}_x}$,$\bar{\Delta}_{\mathbf{n}_y}$, and $\bar{\Delta}_{\mathbf{n}_z}$ the error functional

$$e(\bar{\Delta}_{\mathbf{n}_x}, \bar{\Delta}_{\mathbf{n}_y}, \bar{\Delta}_{\mathbf{n}_z}) = \int_\Omega \left(\langle \hat{\bar{\mathcal{F}}}_i^{(\mathbf{n}_x)}, \hat{\bar{\mathcal{F}}}_i^{(\mathbf{n}_x)} \rangle + \langle \hat{\bar{\mathcal{F}}}_i^{(\mathbf{n}_y)}, \hat{\bar{\mathcal{F}}}_i^{(\mathbf{n}_y)} \rangle + \langle \hat{\bar{\mathcal{F}}}_i^{(\mathbf{n}_z)}, \hat{\bar{\mathcal{F}}}_i^{(\mathbf{n}_z)} \rangle\right)^{\frac{1}{2}} \tag{15}$$

in order to improve the mesh size in each direction.

The approach presented in this paper starts from an existing adaptation method for the numerical approximation errors for steady RANS flows, see [1] and the monograph [11]. In order to extend it to LES/hybrid, we try to combine (a) the existing adaptation of mesh for RANS or non-turbulent steady flow with (b) a special adaptation for LES error model built according to the Toosi-Larsson method. Optimal factors are evaluated in the three principal directions of the RANS adapted metric. These factors are then applied to the eigenvalues of the inital RANS metric in order to obtain the corrected RANS-LES metric. Focusing on hybrid modeling, we anticipate (i) a rather good quasi-convergent capturing in RANS regions, to be combined with (ii) a suffficiently predictive resolution in LES region.

In this work, we focus on flows which are of a somewhat intermediate difficulty. These turbulent flows are assumed to be quasi-periodic with a rather well identified Strouhal number, and possibly quasi-steady in a large part of the computational domain. For a thin airfoil at small angle of attack for example, RANS calculation will produce a steady flow. VLES and hybrid RANS/LES calculations with medium meshes will produce a flow which is mainly steady, generally modeled with RANS, for which a deterministic adaptation criterion will be applied, but which presents also an unsteady region with vortices, where LES modeling applies, and for which a LES-based adaptation criterion must be applied.

2 Modeling

2.1 Navier-Stokes model

The compressible Navier-Stokes equations for mass, momentum and energy conservation read:

$$\mathcal{NS}(W) = 0 \quad + \quad \text{Initial and boundary conditions} \tag{16}$$

where $\mathcal{NS}(W) = 0$ holds for:

$$\left\{ \begin{array}{rcl} \dfrac{\partial \rho}{\partial t} + \nabla \cdot (\rho \mathbf{u}) & = & 0\,, \\ \dfrac{\partial(\rho \mathbf{u})}{\partial t} + \nabla \cdot (\rho \mathbf{u} \otimes \mathbf{u}) + \nabla p - \nabla \cdot \mathcal{T} & = & 0\,, \\ \dfrac{\partial(\rho E)}{\partial t} + \nabla \cdot ((\rho E + p)\mathbf{u}) - \nabla \cdot (\mathcal{T} \cdot \mathbf{u}) + \nabla \cdot (\lambda \nabla T) & = & 0\,, \end{array} \right. \tag{17}$$

where ρ denotes the density (kg/m^3), $\mathbf{u}$ the velocity (m/s), E the total energy per mass (m^2/s^2), p the pressure (N/m^2), given by: $p = (\gamma-1)\big(\rho E - \frac{1}{2}\rho|\mathbf{u}|^2\big)$ with $\gamma = 1.4$, T the temperature (K) such that $\rho C_v T = E - \frac{1}{2}\rho(u^2+v^2+w^2)$, $\lambda = \mu C_p/Pr$ (C_v being the specific heat at constant volume, μ the dynamic viscosity, C_p the specific heat at constant pressure, Pr the Prandtl number). $\mathcal{T}$ is the laminar stress tensor:

$$\mathcal{T} = \mu \left[(\nabla \mathbf{u} + \nabla \mathbf{u}^{\mathrm{T}}) - \frac{2}{3} \nabla .\, \mathbf{u}\, I \right] ,$$

where (in 3D) $\mathbf{u} = (u, v, w)$, μ the laminar dynamic viscosity ($kg/(m.s)$) and λ the laminar thermal conductivity.

2.2 LES model

We have now to recall the LES analysis for the compressible model. For this we recall some notations. The filtered Navier-Stokes equations are considered. The density Favre filter $\tilde{f} = \overline{(\rho f)}/(\bar{\rho})$ (where the over-line denotes the gris filter) is applied and its solution is denoted $\bar{\rho}, \tilde{u}, \tilde{v}, \tilde{w}, \tilde{e}$.

The filtering of compressible Navier-Stokes equations gives the motion of large structures:

$$\frac{\partial\bar\rho}{\partial t}+\frac{\partial(\bar\rho\tilde u_j)}{\partial x_j}=0$$

$$\frac{\partial(\bar\rho\tilde u_i)}{\partial t}+\frac{\partial(\bar\rho\tilde u_i\tilde u_j)}{\partial x_j}=-\frac{\partial\bar p}{\partial x_i}+\frac{\partial(\mu\tilde P_{ij})}{\partial x_j}-\frac{\partial M_{ij}^{(1)}}{\partial\partial x_j}+\frac{\partial M_{ij}^{(2)}}{\partial x_j}$$

$$\frac{\partial(\bar\rho\tilde E)}{\partial t}+\frac{\partial[(\bar\rho\tilde E+\bar p)\tilde u_j]}{\partial x_j}=\frac{\partial(\tilde u_j\tilde\sigma_{ij})}{\partial x_i}-\frac{\partial\tilde q_j}{\partial x_j}+\frac{\partial}{\partial x_j}\Big(E_j^{(1)}+E_j^{(2)}+E_j^{(3)}\Big)$$

in which:

- $\tilde q$ is the resolved heat vector flux, $\tilde q=-k\ grad(\tilde T)$ where k is the heat conductivity and $\tilde T$ is the Favre filtered temperature,

- $E_j^{(1)}, E_j^{(2)}, E_j^{(3)}$ are defined e.g. in [9], $E_j^{(2)}, E_j^{(3)}$ are negligible compared to $E_j^{(1)}$ and the effect of $E_j^{(1)}$ will be neglected in the sequel,

- $M_{ij}^{(1)}$ is defined from the filtering of the convective term in the moment equation:

$$\frac{\overline{\partial(\rho u_i u_j)}}{\partial x_j}=\frac{\partial(\bar\rho\tilde u_i\tilde u_j)}{\partial x_j}+\frac{\partial M_{ij}^{(1)}}{\partial x_j}\quad\Rightarrow\quad M_{ij}^{(1)}=\overline{\rho u_i u_j}-\bar\rho\tilde u_i\tilde u_j. \tag{18}$$

- $M_{ij}^{(2)}$ is defined by:

$$M_{ij}^{(2)}=\overline{\mu P_{ij}}-\mu\tilde P_{ij}\quad with\quad P_{ij}=2S_{ij}-\frac{2}{3}S_{kk}\delta_{ij} \tag{19}$$

where $S_{ij}=\frac{1}{2}(\frac{\partial u_i}{\partial x_j}+\frac{\partial u_j}{\partial x_i})$. As a consequence the resolved strain tensor is denoted by:

$$\widetilde{S_{ij}}=\frac{1}{2}(\frac{\partial\tilde u_i}{\partial x_j}+\frac{\partial\tilde u_j}{\partial x_i})$$

and the viscous term is written

$$\tilde\sigma=\mu\widetilde{P_{ij}}\ \text{ with }\ \widetilde{P_{ij}}=2\widetilde{S_{ij}}-\frac{2}{3}\widetilde{S_{kk}}\delta_{ij}. \tag{20}$$

$M_{ij}^{(2)}$ is negligible compared to $M_{ij}^{(1)}$. The isotropic part of $M_{ij}^{(1)}$, namely $\frac{1}{3}M_{kk}^{(1)}\delta_{ij}$, can be neglected, [12], and its deviatoric part is defined by:

$$T_{ij}=M_{ij}^{(1)}-\frac{1}{3}M_{kk}^{(1)}\delta_{ij}=-\mu_{SGS}\tilde P_{ij}=-\mu_{SGS}\Big(2\widetilde{S_{ij}}-\frac{2}{3}\widetilde{S_{kk}}\delta_{ij}\Big).$$

In our theoretical development, the turbulent viscosity is defined according to Smagorinsky model [25]:

$$\mu_{SGS} = \bar{\rho}(C_s\bar{\Delta})^2|\tilde{S}| \ \text{ with } \ |\tilde{S}| = \sqrt{2\tilde{S}_{ij}\tilde{S}_{ij}} \tag{21}$$

and the model stress tensor is analogous to the one introduced in (5) for the incompressible case:

$$\tau_{ij}^{model} = T_{ij} = -\bar{\rho}(C_s\bar{\Delta})^2|\tilde{S}|\tilde{P}_{ij}. \tag{22}$$

In order to define a Large Eddy Simulation (LES) model from the above one, we restrict to the usual definition of the grid size Δ_g (cf. (1)). We replace in the viscous term of moment equation the viscosity μ by the incremented viscosity $\mu + \mu_{SGS}$. We restrict to quasi-isothermal flows and then we do not introduce a model in the energy equation. Our LES model writes:

$$\mathcal{NS}(W) = \begin{pmatrix} 0 \\ \nabla\cdot\mu_{SGS}\left[(\nabla\mathbf{u} + \nabla\mathbf{u}^{\mathrm{T}}) - \frac{2}{3}\nabla\cdot\,\mathbf{u}\,I\right] \\ 0 \end{pmatrix}. \tag{23}$$

2.3 Spalart-Allmaras model and DDES

Various forms of the Spalart-Allmaras (SA) turbulence model exist. The original Spalart-Allmaras one equation turbulence model writes [27]:

$$\begin{aligned}\frac{\partial\tilde{\nu}}{\partial t} + \mathbf{u}\cdot\nabla\tilde{\nu} &= c_{b1}[1 - f_{t2}]\tilde{S}\tilde{\nu} - \left[c_{w1}f_w - \frac{c_{b1}}{\kappa^2}f_{t2}\right]\left(\frac{\tilde{\nu}}{d}\right)^2 \\ &+ \frac{1}{\sigma}\left[\nabla\cdot((\nu+\tilde{\nu})\nabla\tilde{\nu}) + c_{b2}\|\nabla\tilde{\nu}\|^2\right] + f_{t1}\Delta\mathbf{u}^2\,.\end{aligned}$$

where $\tilde{\nu}$ is the kinematic eddy turbulent viscosity. In this paper we consider the simplified formulation considering $f_{t1} = 0$ and $f_{t2} = 0$:

$$\frac{\partial\rho\tilde{\nu}}{\partial t} + \frac{\partial u_j\rho\tilde{\nu}}{\partial x_j} = \rho c_{b1}\tilde{S}\tilde{\nu} - \rho c_{w1}f_w\left(\frac{\tilde{\nu}}{d}\right)^2 + \frac{\rho}{\sigma}\left[\frac{\partial}{\partial x_j}\left((\nu+\tilde{\nu})\frac{\partial\tilde{\nu}}{\partial x_j}\right) + c_{b2}\frac{\partial\tilde{\nu}}{\partial x_i}\frac{\partial\tilde{\nu}}{\partial x_i}\right].$$

The turbulent eddy viscosity is computed from:

$$\mu_t = \rho\tilde{\nu}f_{v1}$$

where

$$f_{v1} = \frac{\chi^3}{\chi^3 + c_{v1}^3} \quad \text{and} \quad \chi = \frac{\tilde{\nu}}{\nu} \quad \text{with} \quad \nu = \frac{\mu}{\rho}\,.$$

Additional definitions are given by the following equations:

$$\tilde{S} = \Omega + \frac{\tilde{\nu}}{\kappa^2 d^2} f_{v2} \quad \text{where} \quad \Omega = \|\nabla \times \mathbf{u}\|\,.$$

The magnitude of the vorticity is computed from the vorticity tensor where each component is given by $\omega_{ij} = \frac{1}{2}\left(\frac{\partial u_i}{\partial x_j} - \frac{\partial u_j}{\partial x_i}\right)$ and $\Omega = \sqrt{2\sum_{i,j=1..3} \omega_{ij}\omega_{ij}}$. Symbol d holds for the distance from the field point to the nearest wall and

$$f_{v2} = 1 - \frac{\chi}{1 + \chi f_{v1}}\;.$$

Notice that we have the following relations:

$$\chi f_{v1} = \frac{\tilde{\nu} f_{v1}}{\nu} = \frac{\nu_t}{\nu} \quad \Longrightarrow \quad 1 - \frac{\chi}{1 + \chi f_{v1}} = 1 - \frac{\tilde{\nu}}{\nu + \nu_t}\,.$$

The constants are

$$\begin{array}{llll} \sigma = \dfrac{2}{3} & c_{b1} = 0.1355 & c_{b2} = 0.622 & \kappa = 0.41 \\ c_{w1} = \dfrac{c_{b1}}{\kappa} + \dfrac{1 + c_{b2}}{\sigma} & c_{w2} = 0.3 & c_{w3} = 2 & c_{v1} = 7.1\,. \end{array}$$

Finally, the function f_w is computed as:

$$f_w = g\left(\frac{1 + c_{w3}^6}{g^6 + c_{w3}^6}\right)^{1/6} \quad \text{with} \quad g = r + c_{w2}\left(r^6 - r\right) \quad \text{and} \quad r = \min\left(\frac{\tilde{\nu}}{\tilde{S}\kappa^2 d^2}\,,\,10\right)\,.$$

The standard SA one-equation model reads in pseudo-vector notations:

$$\begin{aligned} \frac{\partial \tilde{\nu}}{\partial t} + u_j \frac{\partial \tilde{\nu}}{\partial x_j} &= c_{b1}[1 - f_{t2}]\tilde{S}\tilde{\nu} - \left[c_{w1} f_w - \frac{c_{b1}}{\kappa^2} f_{t2}\right]\left(\frac{\tilde{\nu}}{d}\right)^2 \\ &\quad + \frac{1}{\sigma}\left[\frac{\partial}{\partial x_j}\left((\nu + \tilde{\nu})\frac{\partial \tilde{\nu}}{\partial x_j}\right) + c_{b2}\frac{\partial \tilde{\nu}}{\partial x_i}\frac{\partial \tilde{\nu}}{\partial x_i}\right] \end{aligned}$$

where $f_{t2} = c_{t3}\exp\left(-c_{t4}\chi^4\right)$ with $c_{t3} = 1.2$ and $c_{t4} = 0.5$.

The DDES model [26] replaces the distance d by:

$$\tilde{d} = d - f_d \; max[0, (d - C_{DES}\Delta)]$$

in which $C_{DES} = 0.65$ and with ($\kappa = 0.41$)

$$f_d = 1 - tanh\Big([8r_d]^3\Big) \quad \text{where} \quad r_d = \frac{\nu + \nu_t}{\sqrt{\frac{\partial u_i}{\partial x_j}\frac{\partial u_i}{\partial x_j}}\kappa^2 d^2}.$$

$f_d = 0$ yields RANS while $r_d \ll 1$ yields the LES region.

The above DDES system is denoted in a compact way as :

$$\Psi_{DDES}(W) = 0 \tag{24}$$

where $W = (\rho, \rho u, \rho v, \rho w, \rho E, \rho\tilde{\nu})$ and

$$\begin{aligned}&(\Psi_{DDES}(W), \varphi) = \\ &\int_0^T \int_\Omega \varphi\big[W_t + \mathcal{S}_{DDES}(W) + div\mathcal{F}_{DDES}(W)\big]\mathrm{d}x\mathrm{d}t \\ &+ \int_0^T \int_{\partial\Omega} \varphi\overline{\mathcal{F}}_{DDES}(W)\mathrm{d}\sigma\mathrm{d}t\end{aligned} \tag{25}$$

where $\mathcal{S}_{DDES}(W)$, $\mathcal{F}_{DDES}(W)$, $\overline{\mathcal{F}}_{DDES}(W)$ hold respectively for the source term, the flux and the boundary flux of the DDES model.

3 Mesh-adaptation

In this first study, the focus is on flows which are essentially steady, with a rather small region of the computational domain in which we have a quasi periodic vortex shedding.

In the goal oriented option, we observe that the numerical error $\delta W = W - W_h$ on state variable W can be approximated by the solution of a linearized system

$$A\delta W_{space-time} = S_{space-time}$$

where:
- the linear operator A is the derivative of the Navier-Stokes (resp. URANS, or DDES) residual with respect to the state,
- the right-hand side $S_{space-time}$ of the system is the local error resulting from the space-time discretization (expressed in terms of the metric).

For minimizing the numerical error on the functional $j = (g, W)$ with respect to the mesh metric $\mathcal{M}$, it is sufficient to minimize the product of the adjoint state W^* with the right-hand side,

$$\delta j = (W^*, S_{space-time}),$$

in other words:

$$\text{Find} \quad \mathcal{M}_1 = Arg \min_{\mathcal{M}} \delta j = Arg \min_{\mathcal{M}} (W^*, S_{space-time}(\mathcal{M})). \qquad (26)$$

Similarly, assume that we have also a linear equation for the (test-filtered) error resulting from the LES modeling

$$A\delta W_{LES} = S_{LES}$$

where:
- the linear operator A is again the derivative of the Navier-Stokes residual with respect to the state,
- the right-hand side S_{LES} of the system, the local error of LES, is the divergence of the Germano expression.

As a result, the optimal mesh metric minimizing the total numerical *and* LES error on the functional writes:

$$\mathcal{M}_{both} = Arg \min_{\mathcal{M}} (W^*, S_{space-time}(\mathcal{M}) + S_{LES}(\mathcal{M})). \qquad (27)$$

In this formulation, $S_{space-time}(\mathcal{M})$ and $S_{LES}(\mathcal{M})$ are not necessarily positive and therefore compensations of one error by the other one are possible and can be taken into account in the minimization.

However, up to now, we have not found a satisfying way for expressing explicitly S_{LES} as a function of $\mathcal{M}$ and therefore we cannot apply the strategy producing (27).

In this paper, we shall separate the error analysis into two steps, namely:
(a) research the RANS-optimal metric and,
(b) research of a somewhat LES-optimal metric factor by defining the test filter directions $(\mathbf{n}_k, k = 1, 3$ from the RANS-optimal metric and then follow the Toosi-Larsson for computing the optimal filter widths in these directions.

3.1 Riemannian metric

In the sequel, any mesh is represented by a Riemannian metric. See [1] and [11] for more details on this approach. The Riemannian metric $(\mathcal{M}(\mathbf{x}))_{\mathbf{x}\in\Omega}$ is a symmetric positive matrix 3×3 field defined on the computational domain:

$$\mathcal{M}:\ \mathbf{x}\in\Omega \mapsto \mathcal{M}(\mathbf{x}) \quad = \quad \mathcal{R}(\mathbf{x})\,\Lambda(\mathbf{x})\,{}^t\mathcal{R}(\mathbf{x}), \tag{28}$$

where diagonal matrix $\Lambda(\mathbf{x})$ is

$$\begin{bmatrix} \lambda_1(\mathbf{x}) & & \\ & \lambda_2(\mathbf{x}) & \\ & & \lambda_3(\mathbf{x}) \end{bmatrix} \quad = \quad \begin{bmatrix} h_1^{-2}(\mathbf{x}) & & \\ & h_2^{-2}(\mathbf{x}) & \\ & & h_3^{-2}(\mathbf{x}) \end{bmatrix}. \tag{29}$$

$\mathcal{R}(\mathbf{x})$ is an orthonormal matrix providing the local orientation of mesh stretching through the eigenvectors $(\mathbf{v}_i(\mathbf{x}))_{i=1,3}$, $(\lambda_i(\mathbf{x}))_{i=1,3}$ are the local eigenvalues. $(h_i(\mathbf{x}))_{i=1,3} = (\lambda_i(\mathbf{x})^{-\frac{1}{2}})_{i=1,3}$ are the local mesh sizes along the *principal directions* $\mathbf{p}_{1,\mathcal{M}}, \mathbf{p}_{2,\mathcal{M}}, \mathbf{p}_{3,\mathcal{M}}$ of $\mathcal{M}$ defined by:

$$\mathbf{p}_{k,\mathcal{M}}(\mathbf{x}) \quad = \quad \mathcal{R}(\mathbf{x})\,\mathbf{e}_k\,{}^t\mathcal{R}(\mathbf{x}) \tag{30}$$

where $\mathbf{e}_1, \mathbf{e}_2, \mathbf{e}_3$ are the three Cartesian unitary vectors in x, y, z directions. The density d (number of continuous vertices per unit of volume) of $\mathcal{M}$ is defined from its eigenvalues as

$$d(\mathbf{x}) = det\big(\mathcal{M}(\mathbf{x})\big)^{\frac{1}{2}} = (\lambda_1(\mathbf{x})\,\lambda_2(\mathbf{x})\,\lambda_3(\mathbf{x}))^{\frac{1}{2}} = (h_1(\mathbf{x})\,h_2(\mathbf{x})\,h_3(\mathbf{x}))^{-1}\,.$$

We decompose $\mathcal{M}$ as follows:

$$\mathcal{M}(\mathbf{x}) = d^{\frac{2}{3}}(\mathbf{x})\,\mathcal{R}(\mathbf{x}) \begin{bmatrix} r_1^{-\frac{2}{3}}(\mathbf{x}) & & \\ & r_2^{-\frac{2}{3}}(\mathbf{x}) & \\ & & r_3^{-\frac{2}{3}}(\mathbf{x}) \end{bmatrix} {}^t\mathcal{R}(\mathbf{x})$$

where the r_i's define the stretching strength and where the density d controls the local level of accuracy of $\mathcal{M}$. The *complexity* $\mathcal{C}$ of $\mathcal{M}$, refering to the computational cost is defined as the total number of continuous vertices in the computational domain:

$$\mathcal{C}(\mathcal{M}) = \int_\Omega d(\mathbf{x})\, d\mathbf{x} = \int_\Omega \sqrt{\det(\mathcal{M}(\mathbf{x}))}\, d\mathbf{x}.$$

A discrete tetrahedrization $\mathcal{H}$ is *a unit mesh* for the metric $\mathcal{M}$ if any of its edges **ab** has a length in the metric sufficiently close to unity :

$$\frac{1}{\sqrt{2}} \le \int_0^1 \sqrt{{}^t\mathbf{ab}\; \mathcal{M}(\mathbf{a} + t\,\mathbf{ab})\;\mathbf{ab}}\; \mathrm{d}t \le \sqrt{2}$$

Lastly, we call *refinement* the process which replaces a unit mesh of a given metric $\mathcal{M}$ with local mesh size $(h_1(\mathbf{x})\, h_2(\mathbf{x})\, h_3(\mathbf{x}))$ by a unit mesh of $\mathcal{M}/\beta^2$ with local mesh size $(\beta h_1(\mathbf{x})\, \beta h_2(\mathbf{x})\, \beta h_3(\mathbf{x}))$ and complexity $\mathcal{C}(\mathcal{M}/\beta^2) = \beta^3\mathcal{C}(\mathcal{M})$ where refinement factor β is smaller than one [1] .

3.2 Adaptation sensor for compressible flow

3.2.1 Feature-based adaptation sensor

In the case of a steady RANS calculation of a compressible flow, an efficient approach is to minimize the L^4 norm of interpolation error on the Mach number [1][11]. The local interpolation error $e_\mathcal{M}$ (31) is evaluated in terms of the Hessian H_M of Mach number M and of the metric $\mathcal{M}$ used for generating the mesh:

$$e_\mathcal{M}(\mathbf{x}) = (M - \pi_\mathcal{M} M)(\mathbf{x}) \;=\; \frac{1}{10}\, \mathit{trace}\big(\mathcal{M}(\mathbf{x})^{-\frac{1}{2}}\, |H_M(\mathbf{x})|\, \mathcal{M}(\mathbf{x})^{-\frac{1}{2}}\big), \quad (31)$$

[1] For $\beta = 2$ this refinement is equivalent to dividing mesh size by a factor 2 and multiplying the number of vertices in 3D by a factor 8.

in which $\mathbf{x} \in \Omega$, $(\mathbf{v}_i)_{i=1,3}$ are the local eigen-directions of $\mathcal{M}$, and $(h_i)_{i=1,3}$ are the local sizes of $\mathcal{M}$ along these directions. This local error [2] is a spatially second-order error. In order to take into account boundary layers in good conditions, it has been observed (see again [1] [11]) that the error norm to be minimized is an L^4 norm. The mesh adaptation problem is then written:

$$\text{Find } \mathcal{M}_1 = Arg \min_{\mathcal{M}} \int_\Omega \Big(trace\big(\mathcal{M}(\mathbf{x})^{-\frac{1}{2}}\, |H_M(\mathbf{x})|\, \mathcal{M}(\mathbf{x})^{-\frac{1}{2}}\big)\Big)^4 \mathrm{d}\Omega \qquad (32)$$

under the constraint that the complexity, or integral of the metric density is equal to a specified number N:

$$\mathcal{C}(\mathcal{M}) = \int_\Omega d(\mathcal{M})\mathrm{d}\Omega = N.$$

Expressing via (31) the functional (32) in terms of H_M and assuming that this Hessian is sufficiently smooth, the solution of this constrained optimisation problem can be explicitly computed [1][11]:

$$\mathcal{M}_1 = D_1\ \det(|H_M|)^{\frac{-1}{11}}\, |H_M|,\ \text{with } D_1 = N^{\frac{2}{3}} \left(\int_\Omega \det(|H_M|)^{\frac{4}{11}} \mathrm{d}\Omega \right)^{-\frac{2}{3}}.(33)$$

3.2.2 Goal-oriented adaptation sensor

We consider the Goal Oriented unsteady formulation as it is introduced in [7] and its extension to RANS as presented in [6, 11]. We keep the notations of these papers. We want to minimize the error $(g, W - W_h)$ committed in the approximation of the functional (or scalar output):

$$j = (g, W),$$

where W is the exact solution of the state equation (24,25) and W_h the approximate solution. Let us introduce the adjoint state W^*, solution of the adjoint system:

$$\Big(\frac{\partial \Psi_{DDES}}{\partial W}\Big)^* W^* = g. \qquad (34)$$

[2] $e_{\mathcal{M}}$ is an *a priori* error when we consider that M is the exact Mach number field. In practice, it will be an *a posteriori* error since $e_{\mathcal{M}}$ will be computed from a discrete solution through a recovery technique.

We reproduce now in short the error estimate developed in [19],[7],[6][2]. The functional error estimates writes:

$$|(g, W_h - W)| \approx \mathcal{E}^p_{\text{space}}(\mathcal{M}) \tag{35}$$

with

$$\begin{aligned} &\mathcal{E}^p_{\text{space}}(\mathcal{M}) \approx \\ &\int_0^T \int_\Omega |W^*| |\big(W - \pi_{\mathcal{M}} W\big)_t + \mathcal{S}_{DDES}(W) - \pi_{\mathcal{M}} \mathcal{S}_{DDES}(W)\big)| \, \mathrm{d}x \, \mathrm{d}t \\ &\qquad + \int_0^T \int_\Omega |\frac{\partial \mathcal{F}_{DDES}}{\partial W} \cdot \nabla W^*| \;\; |W - \pi_{\mathcal{M}} W| \mathrm{d}x \, \mathrm{d}t \\ &\qquad + \int_0^T \int_\Gamma |W^*| \;\; |(\bar{\mathcal{F}}_{DDES}(W) - \pi_{\mathcal{M}} \bar{\mathcal{F}}_{DDES}(W)) \cdot \mathbf{n}| \, \mathrm{d}\Gamma \, \mathrm{d}t. \end{aligned}$$

Neglecting the boundary term, we get:

$$\mathcal{E}_{\text{space}}(\mathcal{M}) \;\; \approx \;\; \int_0^T \int_\Omega \text{trace}\left(\mathcal{M}^{-\frac{1}{2}}(\mathbf{x}, t) \, \mathbf{H}(\mathbf{x}, t) \, \mathcal{M}^{-\frac{1}{2}}(\mathbf{x}, t)\right) \, \mathrm{d}x \, \mathrm{d}t, \tag{36}$$

$$\text{with} \quad \mathbf{H}(\mathbf{x}, t) = |W^*_t + W^* \frac{\partial \mathcal{S}_{DDES}}{\partial W} + \frac{\partial \mathcal{F}_{DDES}}{\partial W} \cdot \nabla W^*| \;\; |H(W)|, \tag{37}$$

where $H(W)$ is the Hessian of W.

Lemma 3.1. Unified numerical error criterion. *The two numerical error criteria, namely (31,32,33) for the feature-based option and (35,36,37) for the Goal-Oriented option, examined previously, and the related optimization problems can be unified as follows:*

$$\begin{aligned} &\mathcal{M}_{num}(\mathbf{x}) = \mathcal{R}_{num}(\mathbf{x}) \begin{bmatrix} h_{1,num}(\mathbf{x}) & & \\ & h_{2,num}(\mathbf{x}) & \\ & & h_{3,num}(\mathbf{x}) \end{bmatrix} {}^t\mathcal{R}_{num}(\mathbf{x}) \\ &\mathcal{M}_{num} = \mathit{Argmin} \; \mathcal{E}(\mathcal{M}) = \mathit{Argmin} \int_0^T \mathcal{E}_{\text{space},t}(\mathcal{M}, t) \, \mathrm{d}t \quad \mathit{with} \\ &\mathcal{E}_{\text{space},t}(\mathcal{M}, t) = \int_\Omega \left[\text{trace}\left(\mathcal{M}^{-\frac{1}{2}}(\mathbf{x}, t) \, \mathbf{H}(\mathbf{x}, t) \, \mathcal{M}^{-\frac{1}{2}}(\mathbf{x}, t)\right)\right]^p \mathrm{d}x, \end{aligned} \tag{38}$$

where :

- *in the Feature-Based case, a sensor M is computed from W, setting $\mathbf{H} = H_M$.*

- *in the Goal-Oriented case, $p = 1$, and W^* is the adjoint state, $\mathbf{H}$ is defined as in (37).*

Since the flow of interest is quasi-steady in a large part of the computational domain, we keep the metric $\mathcal{M}_{num}$ resulting from the optimization of the numerical error functional $\mathcal{E}(\mathcal{M})$ as a basis for the proposed extension to LES/DDES.

3.3 Toosi-Larsson adaptation step

A simplified way to explain the Toosi-Larsson method [28] is to consider:
- an anisotropic Cartesian mesh available with Cartesian directions $\mathbf{n}_x, \mathbf{n}_y, \mathbf{n}_z$,
- three test filters evaluated on the flow in these three directions,
- then new local mesh sizes in these directions $\Delta x(\mathbf{x}, \mathbf{n}_x)$, $\Delta y(\mathbf{x}, \mathbf{n}_x)$, $\Delta z(\mathbf{x}, \mathbf{n}_x)$, $\mathbf{x} \in \Omega$, are defined, defining a new adapted mesh, with variation of mesh size and stretching, but with the same principal directions.

We propose here an extended approach for the case of a metric-based anisotropic mesh. Let $\mathcal{M}_{num}$ be *one of the two* metrics defined in (38) with local mesh sizes $(h_{1,num}(\mathbf{x}), h_{2,num}(\mathbf{x}), h_{3,num}(\mathbf{x}))$ according to (29) and $\mathcal{H}_{num}$ a unit mesh of $\mathcal{M}_{num}$. We start from a LES or hybrid simulation performed on mesh $\mathcal{H}_{num}$ and using a LES a filter size:

$$\bar{\Delta}_0(\mathbf{x}) = (h_{1,num}(\mathbf{x}) h_{2,num}(\mathbf{x}) h_{3,num}(\mathbf{x}))^{\frac{1}{3}}.$$

Then three test filters are built in principal directions $(\mathbf{p}_k(\mathbf{x})),\ k = 1,3$ of $\mathcal{M}_{num}$ (according to the definition in (30)),

$$\mathbf{n}_k(\mathbf{x}) = \hat{\Delta}_{\mathbf{n}_k}(\mathbf{x}) \mathbf{p}_{k,\mathcal{M}_0}(\mathbf{x}) \tag{39}$$

having the length

$$||\mathbf{n}_k(\mathbf{x})|| = \hat{\Delta}_{\mathbf{n}_k}(\mathbf{x}) = 2\bar{\Delta}(\mathbf{x}) \quad k = 1,3. \tag{40}$$

The test filter width $= \hat{\Delta}_{\mathbf{n}_k}$ will vary in the neighbohood of a reference width:

$$||\mathbf{n}_{k,0}(\mathbf{x})|| = \hat{\Delta}_{\mathbf{n}_{k,0}}(\mathbf{x}) = 2\bar{\Delta}_0(\mathbf{x}) \quad k = 1,3. \tag{41}$$

We consider the effect of the test filter, which we denote $\hat{.}^{(\mathbf{n}_k)}$. The error source term (14) becomes in the compressible case:

$$\widehat{\overline{\mathcal{F}}}_i^{(\mathbf{n}_k)}(\mathbf{x}) = \frac{\partial}{\partial x_j}\Big(\tau_{ij}^{model}(\widehat{\overline{u}}^{(\mathbf{n}_k)}) - \widehat{\tau_{ij}^{model}(\overline{u})}^{(\mathbf{n}_k)} - \mathcal{M}_{ij}\Big). \tag{42}$$

where

$$\mathcal{M}_{ij} = \widehat{\overline{\rho u_i u_j}}^{(\mathbf{n}_k)} - \Big(\frac{\widehat{\overline{\rho u_i}}^{(\mathbf{n}_k)}\widehat{\overline{\rho u_j}}^{(\mathbf{n}_k)}}{\widehat{\overline{\rho}}^{(\mathbf{n}_k)}}\Big) \tag{43}$$

It can be shown [14] that the SGS and the sub-test stress tensors are related by the following identity :

$$\mathcal{L}_{ij} = \widehat{\bar{\rho}\tilde{u}_i\tilde{u}_j}^{(\mathbf{n}_k)} - \frac{1}{\widehat{\bar{\rho}}^{(\mathbf{n}_k)}}\Big(\widehat{\bar{\rho}\tilde{u}_i}^{(\mathbf{n}_k)}\widehat{\bar{\rho}\tilde{u}_j}^{(\mathbf{n}_k)}\Big) = \mathcal{M}_{ij} - \widehat{M_{ij}^{(1)}}^{(\mathbf{n}_k)}. \tag{44}$$

Let us denote

$$L_{ij} = \mathcal{L}_{ij} - \frac{1}{3}\mathcal{L}_{kk}\delta_{ij}. \tag{45}$$

Then, to each test filter $\mathbf{n}_k$ corresponds an error source term

$$\widehat{\overline{\mathcal{F}}}_i^{(\mathbf{n}_k)}(\mathbf{x}) = \frac{\partial}{\partial x_j}\Big(\tau_{ij}^{model}(\widehat{\overline{u}}^{(\mathbf{n}_k)}) - \widehat{\tau_{ij}^{model}(\overline{u})}^{(\mathbf{n}_k)} - L_{ij}\Big). \tag{46}$$

From (44),(45) and (46), we deduce :

Lemma 3.2.

$$\begin{aligned}\widehat{\overline{\mathcal{F}}}_i^{(\mathbf{n}_k)}(\mathbf{x}) \quad &= \quad \frac{\partial}{\partial x_j}\Big((C\bar{\Delta}^2)\widehat{\bar{\rho}|\tilde{S}|\tilde{P}_{ij}}^{(\mathbf{n}_k)} - (C\bar{\Delta}^2)\Big(\frac{\widehat{\Delta}^{(\mathbf{n}_k)}}{\bar{\Delta}}\Big)^2\widehat{\bar{\rho}}^{(\mathbf{n}_k)}|\widehat{\tilde{S}}^{(\mathbf{n}_k)}|\widehat{\tilde{P}_{ij}}^{(\mathbf{n}_k)} \\ &-\widehat{\bar{\rho}\tilde{u}_i\tilde{u}_j}^{(\mathbf{n}_k)} + \tfrac{1}{\widehat{\bar{\rho}}^{(\mathbf{n}_k)}}(\widehat{\bar{\rho}\tilde{u}_i}^{(\mathbf{n}_k)}\widehat{\bar{\rho}\tilde{u}_j}^{(\mathbf{n}_k)}) + \tfrac{1}{3}\Big(\widehat{\bar{\rho}\tilde{u}_l\tilde{u}_l}^{(\mathbf{n}_k)} - \tfrac{1}{\widehat{\bar{\rho}}^{(\mathbf{n}_k)}}(\widehat{\bar{\rho}\tilde{u}_l}^{(\mathbf{n}_k)}\widehat{\bar{\rho}\tilde{u}_l}^{(\mathbf{n}_k)})\Big)\delta_{ij}\Big) \\ &\qquad i = 1, ..., 3, \quad k = 1, ..., 3..\square.\end{aligned} \tag{47}$$

In the Piomelli dynamic formulation, C (or $C\bar{\Delta}^2$) is the unknown scalar parameter to be choosen at each point of the computational domain in order to optimize the efficiency of the LES model. In the present analysis, $C\bar{\Delta}^2$ is known, and the optimization variables are the three filter sizes $\widehat{\Delta}^{(\mathbf{n}_1)}, \widehat{\Delta}^{(\mathbf{n}_2)}, \widehat{\Delta}^{(\mathbf{n}_3)}$. We observe that, when we freeze all the filtered terms, $\widehat{\Delta}^{(\mathbf{n}_k)}$ appears explicitly in (47) under the form of a quadratic term. But for all "hat" filtered quantity, we remark that they approximatively differ from the non-filtered quantity by a rest proportional to the product of square of filter width times a second derivative of unfiltered quantity. However, following [28], and for the sake of simplicity, we work in the neighborhood of a LES filter width $\bar{\Delta}_0$:

$$\widehat{\overline{\mathcal{F}}}_i^{(\mathbf{n}_{k,0})} = \widehat{\overline{\mathcal{F}}}_i^{(\mathbf{n}_k)}|_{\bar{\Delta}=\bar{\Delta}_0,\hat{\Delta}^{(\mathbf{n}_k)}=\hat{\Delta}^{(\mathbf{n}_{k,0})}=2\bar{\Delta}_0}, \quad i = 1, ..., 3, \quad k = 1, ..., 3. \tag{48}$$

In the neighborhood of $\bar{\Delta} = \bar{\Delta}_0, \hat{\Delta}^{(\mathbf{n}_k)} = 2\bar{\Delta}_0$, we approximate the variation of $\widehat{\overline{\mathcal{F}}}_i^{(\mathbf{n}_k)}$ in the neighborhood of $\mathbf{n}_{k,0}$ with the following quadratic formula:

$$\widehat{\overline{\mathcal{F}}}_i^{(\mathbf{n}_k)} \quad \approx \quad \Big(\frac{\hat{\Delta}^{(\mathbf{n}_k)}}{2\ \overline{\Delta}_0}\Big)^2 \widehat{\overline{\mathcal{F}}}_i^{(\mathbf{n}_{k,0})} \qquad i = 1, ..., 3, \quad k = 1, ..., 3, \tag{49}$$

We observe that this approximation of an error term for LES is coherent with the fact that the LES model is obtained by perturbating the Navier-Stokes model by the SGS term which is of second order with respect to the mesh size $\bar{\Delta}$. We introduce the notations:

$$\Delta_k = \frac{\hat{\Delta}^{(\mathbf{n}_k)}}{2} \quad ; \quad \mathcal{G}_k = \bar{\Delta}^{-2}\Big(\langle\widehat{\overline{\mathcal{F}}}^{(\mathbf{n}_{k,0})}, \widehat{\overline{\mathcal{F}}}^{(\mathbf{n}_{k,0})}\rangle\Big)^{\frac{1}{2}} \quad k = 1, ..., 3, \tag{50}$$

where the scalar product $\langle a, b\rangle = \sum_{i=1,3} a_i b_i$. We shall now find the following metric (aligned with numerical metric $\mathcal{M}_{num}$ defined in (38)):

$$\mathcal{M}(\mathbf{x}) = \mathcal{R}_{num}(\mathbf{x}) \begin{bmatrix} (\frac{h_{1,num}}{\bar{\Delta}}\Delta_1)^{-2}(\mathbf{x}) & & \\ & (\frac{h_{2,num}}{\bar{\Delta}}\Delta_2)^{-2}(\mathbf{x}) & \\ & & (\frac{h_{3,num}}{\bar{\Delta}}\Delta_3)^{-2}(\mathbf{x}) \end{bmatrix} {}^t\mathcal{R}_{num}(\mathbf{x})$$

which minimizes the functional:

$$e(\Delta_1, \Delta_2, \Delta_3) = \int_\Omega \Big(\mathcal{G}_1^2\Delta_1^4 + \mathcal{G}_2^2\Delta_2^4 + \mathcal{G}_3^2\Delta_3^4\Big)^{\frac{1}{2}} \mathrm{d}x \tag{51}$$

under the constraint:

$$\mathcal{C}(\mathcal{M}) = N$$

where N is prescribed by the user. We observe that the complexity writes:

$$\mathcal{C}(\mathcal{M}) = \int_\Omega \bar{\Delta}^3 (h_1 h_2 h_3 \Delta_1\Delta_2\Delta_3)^{-1} \mathrm{d}x$$

which reduces the problem to a minimization with respect to $(\Delta_1, \Delta_2, \Delta_3)$ under the constraint that the integral of their product is specified. Let us denote by $(\Delta_1^{opt}, \Delta_2^{opt}, \Delta_3^{opt})$ the solution of the minimization problem and:

$$\zeta^{opt} = \Big(\Delta_1^{opt}\Delta_2^{opt}\Delta_3^{opt}\Big)^{-1}.$$

In any point $\mathbf{x}$, knowing solely ζ^{opt}, we can deduce the Δ_k^{opt}'s since the (squared) value of the integrand

$$g(\mathbf{x}) = \mathcal{G}_1^2(\mathbf{x})\Delta_1^4(\mathbf{x}) + \mathcal{G}_2^2(\mathbf{x})\Delta_2^4(\mathbf{x}) + \mathcal{G}_3^2(\mathbf{x})\Delta_3^4(\mathbf{x})$$

must be minimized with respect to the $((\Delta_1^{opt})^4, (\Delta_2^{opt})^4, (\Delta_3^{opt})^4)$, with the constraint that their product $(\zeta^{opt})^{-4}$ is given. This implies that

$$\begin{aligned} \mathcal{G}_1^2(\mathbf{x})(\Delta_1^{opt})^4(\mathbf{x}) = \mathcal{G}_2^2(\mathbf{x})(\Delta_2^{opt})^4(\mathbf{x}) = \mathcal{G}_3^2(\mathbf{x})(\Delta_3^{opt})^4(\mathbf{x}) = \\ \Big((\zeta^{opt})^{-4}\mathcal{G}_1^2(\mathbf{x})\mathcal{G}_2^2(\mathbf{x})\mathcal{G}_3^2(\mathbf{x})\Big)^{\frac{1}{3}} \end{aligned} \tag{52}$$

or, for $k = 1, 3$:

$$\Delta_k^{opt}(\mathbf{x}) = (\zeta^{opt})^{-\frac{1}{3}}\Big(\mathcal{G}_1(\mathbf{x})\mathcal{G}_2(\mathbf{x})\mathcal{G}_3(\mathbf{x})\Big)^{\frac{1}{6}}\Big(\mathcal{G}_k(\mathbf{x})\Big)^{-\frac{1}{2}}.$$

It remains to minimize

$$\mathcal{K}(\zeta) = \int_\Omega K(\mathbf{x})\zeta^{-\frac{2}{3}}(\mathbf{x})\mathrm{d}x$$

with

$$K(\mathbf{x}) = \Big(\sum_{k=1}^{k=3}\mathcal{G}_k^2\Big(\mathcal{G}_1(\mathbf{x})\mathcal{G}_2(\mathbf{x})\mathcal{G}_3(\mathbf{x})\Big)^{\frac{4}{6}}\Big(\mathcal{G}_k(\mathbf{x})\Big)^{-\frac{4}{2}}\Big)^{\frac{1}{2}}$$

under the constraint $\int_\Omega \zeta(\mathbf{x})\mathrm{d}x = N$. The resolution of this minimization problem gives:

$$K(\mathbf{x})\zeta^{-\frac{5}{3}}(\mathbf{x}) = \mathit{const.} \Rightarrow \zeta(\mathbf{x}) = \mathit{const.}^{-\frac{3}{5}}K(\mathbf{x})^{\frac{3}{5}}$$

$$N = \int_\Omega \zeta\mathrm{d}x = \mathit{const.}^{-\frac{3}{5}}\int_\Omega K^{\frac{3}{5}}\mathrm{d}x \Rightarrow \mathit{const.}^{-\frac{3}{5}} = N\Big(\int_\Omega K^{\frac{3}{5}}\mathrm{d}x\Big)^{-1}$$

$$\zeta^{opt}(\mathbf{x}) = \Big(\int_\Omega K^{\frac{3}{5}}(\mathbf{x}')\mathrm{d}x'\Big)^{-1}K(\mathbf{x})^{\frac{3}{5}}\ N \tag{53}$$

and

$$\Delta_k^{opt}(\mathbf{x}) = \Big(\mathcal{G}_1(\mathbf{x})\mathcal{G}_2(\mathbf{x})\mathcal{G}_3(\mathbf{x})\Big)^{\frac{1}{6}}\Big(\mathcal{G}_k(\mathbf{x})\Big)^{-\frac{1}{2}}\Big(\int_\Omega K^{\frac{3}{5}}(\mathbf{x}')\mathrm{d}x'\Big)^{\frac{1}{3}}K(\mathbf{x})^{-\frac{1}{5}}\ N^{-\frac{1}{3}}. \tag{54}$$

In practice we think it is better that the initial metric $\mathcal{M}_0$ defining the filter should be the metric defining the previous mesh while the test filter directions will be chosen from the novel mean flow adaptation metric $\mathcal{M}_1$. then the metric adapting to both Mach field and LES would write:

$$\mathcal{M}_{H,DDES}(\mathbf{x}) = \mathcal{R}_1(\mathbf{x}) \begin{bmatrix} (\frac{h_1^1\Delta_1}{\Delta})^{-2}(\mathbf{x}) & & \\ & (\frac{h_2^1\Delta_2}{\Delta})^{-2}(\mathbf{x}) & \\ & & (\frac{h_3^1\Delta_3}{\Delta})^{-2}(\mathbf{x}) \end{bmatrix} {}^t\mathcal{R}_1(\mathbf{x}).$$

This step will probably increase the complexity $\mathcal{C}(\mathcal{M}_{H,LES})$ which will be larger than N. A final step of renormalization is then necessary:

$$\mathcal{M}_{H,DDES}^{new} = N^{\frac{2}{3}}\Big(\mathcal{C}(\mathcal{M}_{H,DDES})\Big)^{-\frac{2}{3}}\mathcal{M}_{H,DDES}.$$

4 Space and time approximation

The optimal continuous metric has been obtained as the solution of a continuous non-linear system. In practice, we discretize all continuous ingredients, expressing the dependancy of a discrete flow field $W_{\mathcal{H}}$ to a discrete metric $\mathcal{M}$, via the construction of a unit mesh $\mathcal{H}$ of the metric $\mathcal{M}$ and the solution on the mesh of discrete CFD system to get $W_{\mathcal{H}}$:

$$\mathcal{M} \mapsto \mathcal{H} \mapsto W_{\mathcal{H}}. \tag{55}$$

We use a single mesh for the whole time interval of LES or hybrid computation.

Then we apply to the discrete nonlinear optimality system a fixed point iteration in order to obtain the optimal metric and mesh.

4.1 CFD numerics

The CFD software used in this paper is the NiceFlow software of Lemma. It relies on the *vertex-centered* MUSCL approximation for *tetrahedrizations* described in details in Section 1.2 of [11], see also [6] for the description of a similar computer code. NiceFlow involves the mesh adaptation functionalities ([11],[6]) used in this study: computation of metric-based adaptation criteria, regeneration of adapted anisotropic meshes.

4.2 Implementation of LES criterion

4.2.1 LES filter

The SGS term is assembled by element and the filter size $\bar{\Delta} = (h_1 h_2 h_3)^{\frac{1}{3}}$ is evaluated from the volume of the local element jt:

$$\bar{\Delta}|_{jt} = \big(vol(jt)\big)^{\frac{1}{3}}.$$

4.2.2 Test filter

In [20] an isotropic test filter is built at each vertex is from a mean on the elements jt which have is as vertex, which we write $jt \ni is$:

$$\widehat{w(is)} = \Big(\sum_{jt \ni is} \sum_{js \in jt} vol(jt)\Big)^{-1} \sum_{jt \ni is} \sum_{js \in jt} vol(jt)\; w(js) \tag{56}$$

where the $\sum_{js \in jt}$ means the sum over the vertices js of element jt and $vol(jt)$ holds for the volume of element jt. It results that the integration area of the test filter is the P_1 basis function support, or union of elements around a vertex. Equivalently, the test filter is a mean on the set of neighboring elements, of volume $Vol_{is} = \sum_{jt \ni is} vol(jt)$. Defining as N_{is} the number of elements having vertex is as a vertex, and assuming that the volume of elements around vertex is is close to $vol(jt)$ for a element containing is, then $Vol_{is} \approx N_{is} vol(jt)$. Taking $vol(jt)$ as the integration area of the model filter, we can set:

$$\frac{\hat{\Delta}}{\Delta} = N_{is}^{\frac{1}{3}}.$$

As *anisotropic test filter directions*, we use the principal directions $\mathbf{p}_{k,\mathcal{M}}$ (see (30)) of the background RANS/hybrid metric:

$$\mathbf{n}_k = 2\bar{\Delta}\; \mathbf{p}_{k,\mathcal{M}}.$$

The anisotropic filter according to vector $\mathbf{n}_k$, that is, aligned with the unit vector $\mathbf{p}_{k,\mathcal{M}}$, and of filter width $2\bar{\Delta}$ writes:

$$\widehat{w(is)}^{k} = \sum_{jt \ni is} \sum_{js \in jt} vol(jt) |\langle \frac{\mathbf{isjs}}{|isjs|}, \mathbf{n}_k \rangle|\; w(js) \Big(\sum_{jt \ni is} \sum_{js \in jt} vol(jt) |\langle \frac{\mathbf{isjs}}{|isjs|}, \mathbf{n}_k \rangle|\Big)^{-1} \tag{57}$$

where **isjs** is the vector from vertex is to vertex js.

5 Adaptation algorithm

The adaptation algorithm solves the discretization of the optimality conditions for the optimal metric. The flows under study are unsteady. In order to apply mesh adaptation, we shall use a version of the Transient Fixed Point introduced in [3]. A sketch of this algorithm is given by Algorithm 1.

Algorithm 1 Transient Fixed Point

```
Given a complexity $N_{prescribed}$, an initial metric, $\mathcal{M}_0$ of complexity $c_0$,
build a unit mesh $\mathcal{H}_0$ from $\mathcal{M}_0$
For $iadapt = 0, nadapt$
    • Compute over $[0, T]$ the flow $W_{iadapt}$ from with mesh $\mathcal{H}_{iadapt}$
    • Compute the $k_{max}$ new metrics $\mathcal{M}^k_{iadapt+1}$ of complexity $N_{prescribed}$ each
      taking into account the flow over $[t_k, t_{k+1}]$.
    • Compute the $k_{max}$ new meshes $\mathcal{H}^k_{iadapt+1}$ from $\mathcal{M}^k_{iadapt+1}$
    • $iadapt = iadapt + 1$
End for $iadapt$
```

Let us assume that Algorithm 1 iteratively converges (when *iadapt* increases to infinity) to a fixed point $(W_\infty, \mathcal{M}_\infty)$. Then this fixed point is a numerical flow computed on a succession of meshes $\mathcal{M}^k_\infty, k = 1, k_{max}$, each mesh $\mathcal{H}^k_\infty$ being adapted to the best approximation (in some sense) of the flow on time interval $[t_k, t_{k+1}]$. Further, the sum of the complexities of the different meshes for $k = 1, k_{max}$ is the global complexity $k_{max}N_{prescribed}$.

As in the previous chapter, since we are interested by vortex shedding flows past blunt bodies, we shall work with the *single-mesh option of the transient fixed point*. Indeed, we want to work with only one mesh for the whole time interval, and we put:

$$k_{max} = 1 \ . \tag{58}$$

6 Numerical applications

In this first application of the proposed mesh adaptation method, we concentrate on the flow around a circular cylinder, and in particular on two typical flows, depending of their Reynolds number:
- a typical subcritical flow is the flow a Reynolds number 3900 in which the boundary layer is said a laminar one, while the detached wake is turbulent,
- a typical supercritical flow if Reynolds 1 Million, in which both boundary layers and wake present turbulent characteristic.

Here subcritical and supercritical refer to the drag crisis Reynolds numbers around 300000 at which the drag decreases rapidly.
- a flow past a wing.
- a flow around a tandem cylinder.

6.1 Subcritical flow calculation with adaptation

The subcritical cases are flows around a circular cylinder at Reynolds number 3900 and $20K$. Several computations and measurements are described in Chapter 6. The boundary layer being of laminar regime (although participating to the mechanism of the turbulent global flow), the state-of-art modelisation for this flow is to apply a LES model of medium sophistication. We choose the combination of the VMS formulation with the WALE SGS model, as described in the chapter recalling some turbulence models.

A first mesh-adaptive calculation uses the Hessian of Mach number as anisotropic adaptation criterion, with the L^4 norm, according to the results of available experiments, see for example [**?**]. For the same reasons as for the space-time adaption study of Chapter 8, this unsteady flow is adapted with a mesh unchanged during the time interval , using the single-mesh transient fixed point.

6.1.1 Re = 3900

First, let us take a look at Figure 1 to see what our algorithm produces for $\Delta_1^{\text{opt}}/\bar{\Delta}$. Note that this value varies enormously, from 10^{-4} to 86. Keeping in mind that this value multiplies the local mesh size h_1 we decide to reduce the range of possible values for $\Delta_1^{\text{opt}}/\bar{\Delta}$ (Figure 2).

In the mesh adaptation method of this chapter, the detection of vortices is translated in a field of multiplicative factors of the local mesh size. This field is depicted in Figure 2.

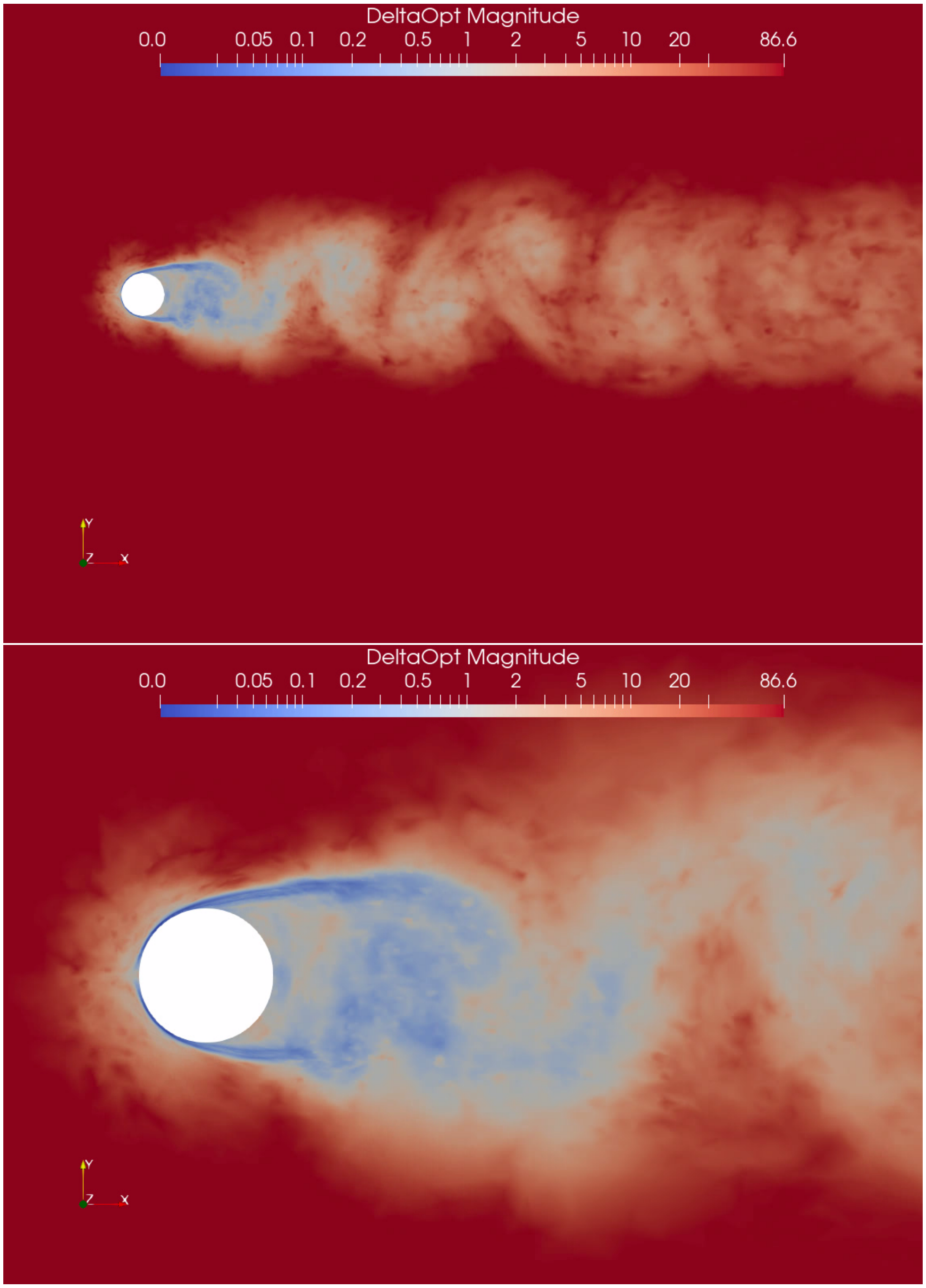

Figure 1: *Instantaneous value of* $\Delta_1^{opt}/\bar{\Delta}$ *for flow around a cylinder at* $Re = 3900$. *These values are those given by the algorithm without clamping.*

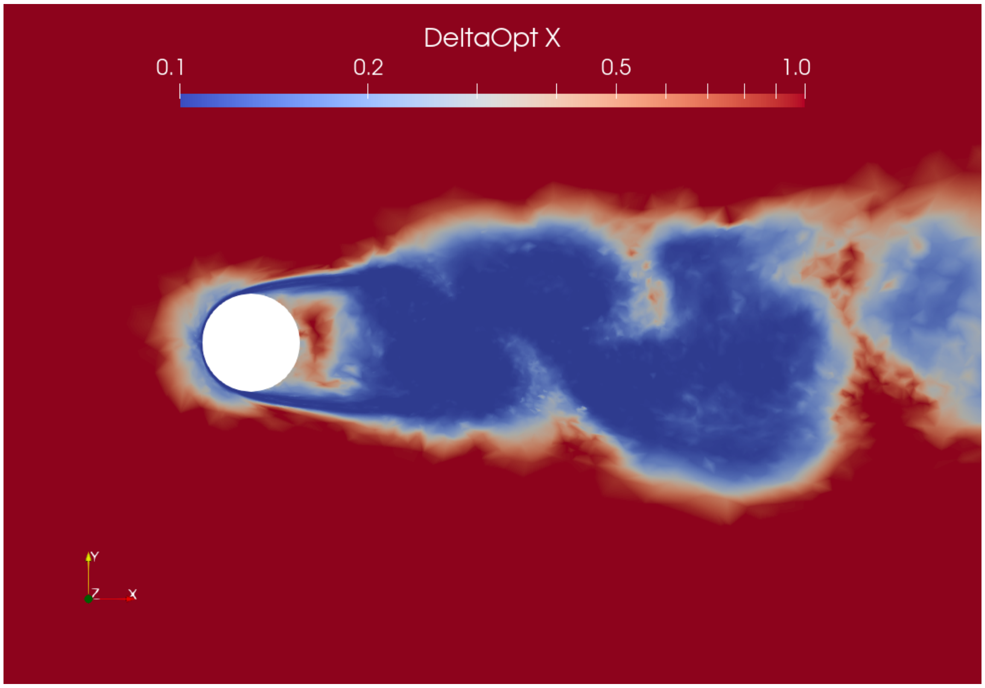

Figure 2: *Instantaneous value of* $\Delta_1^{opt}/\bar{\Delta}$ *for flow around a cylinder at* $Re = 3900$*. These values are those given by the algorithm with a choosen clamping.*

The resulting mesh is presented in Figure 3 where the region one diameter after the cylinder received a supplement of vertices.

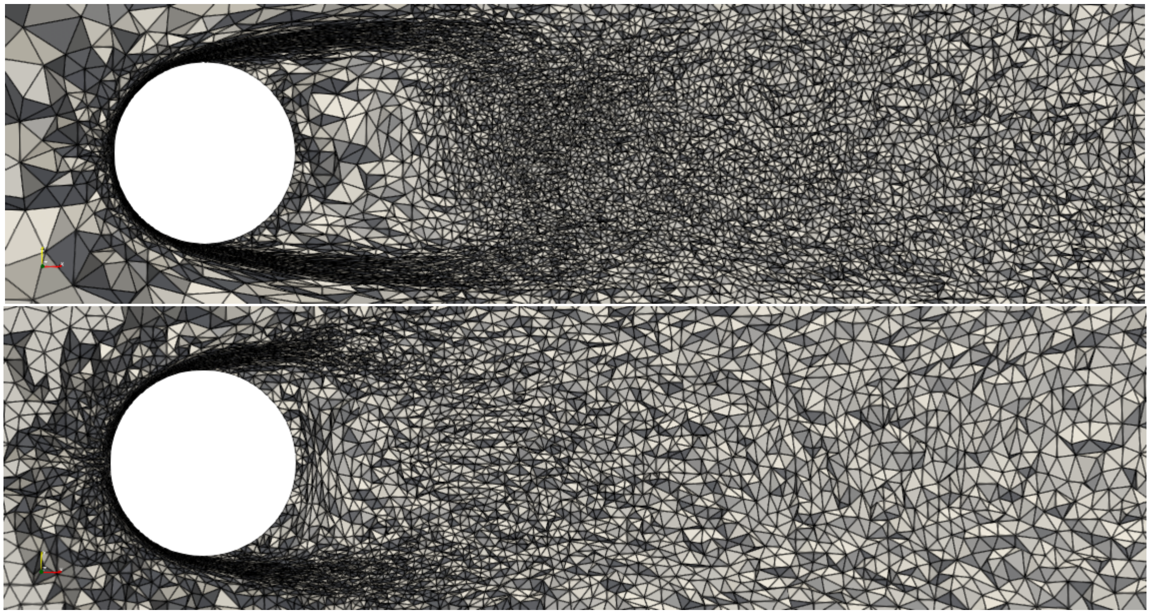

Figure 3: *Cylindre Re = 3900 VMS-WALE results : Top, mesh obtained with the new LES criterion (around 400K vertices), and bottom, mesh obtained with Mach criterion only (around 300K vertices).*

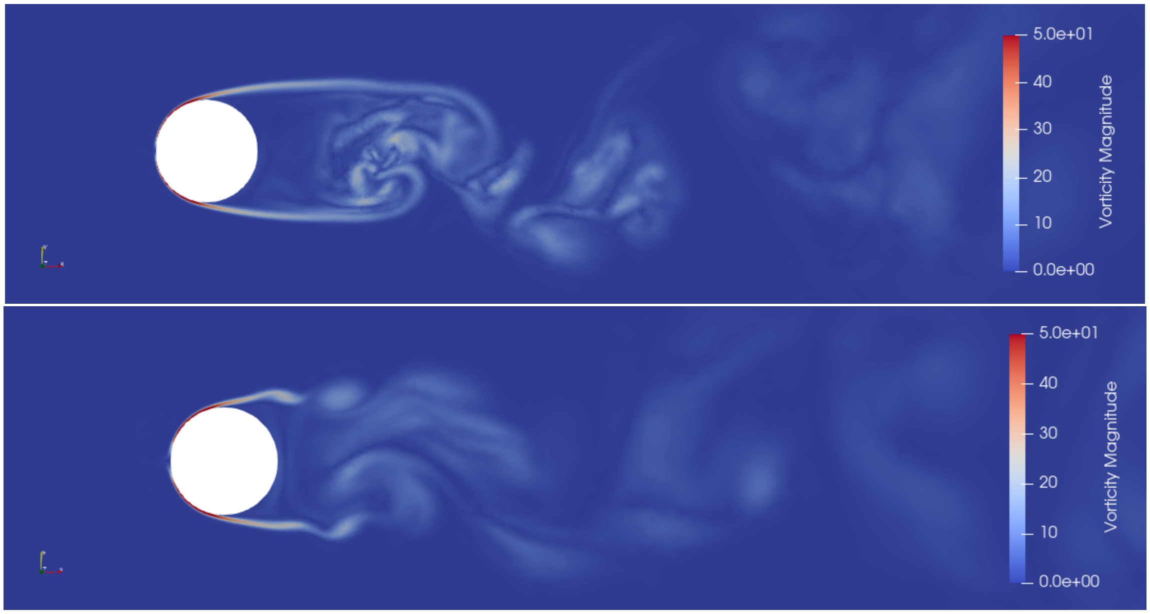

Figure 4: *Cylindre Re = 3900 VMS-WALE results : Top, vorticity obtained with the new LES criterion, and bottom, vorticity obtained with Mach criterion only.*

6.1.2 Re = 20 000

For this test case, we compare the results obtained in Chapter 6 with those obtained for our new method. Looking at the meshes obtained in Figure 6, we do not see any drastic change, even if the back body for the mesh obtained with our new theory seems more remeshed. Nevertheless, Figure 1 shows that our vorticity field is captured with much greater precision.

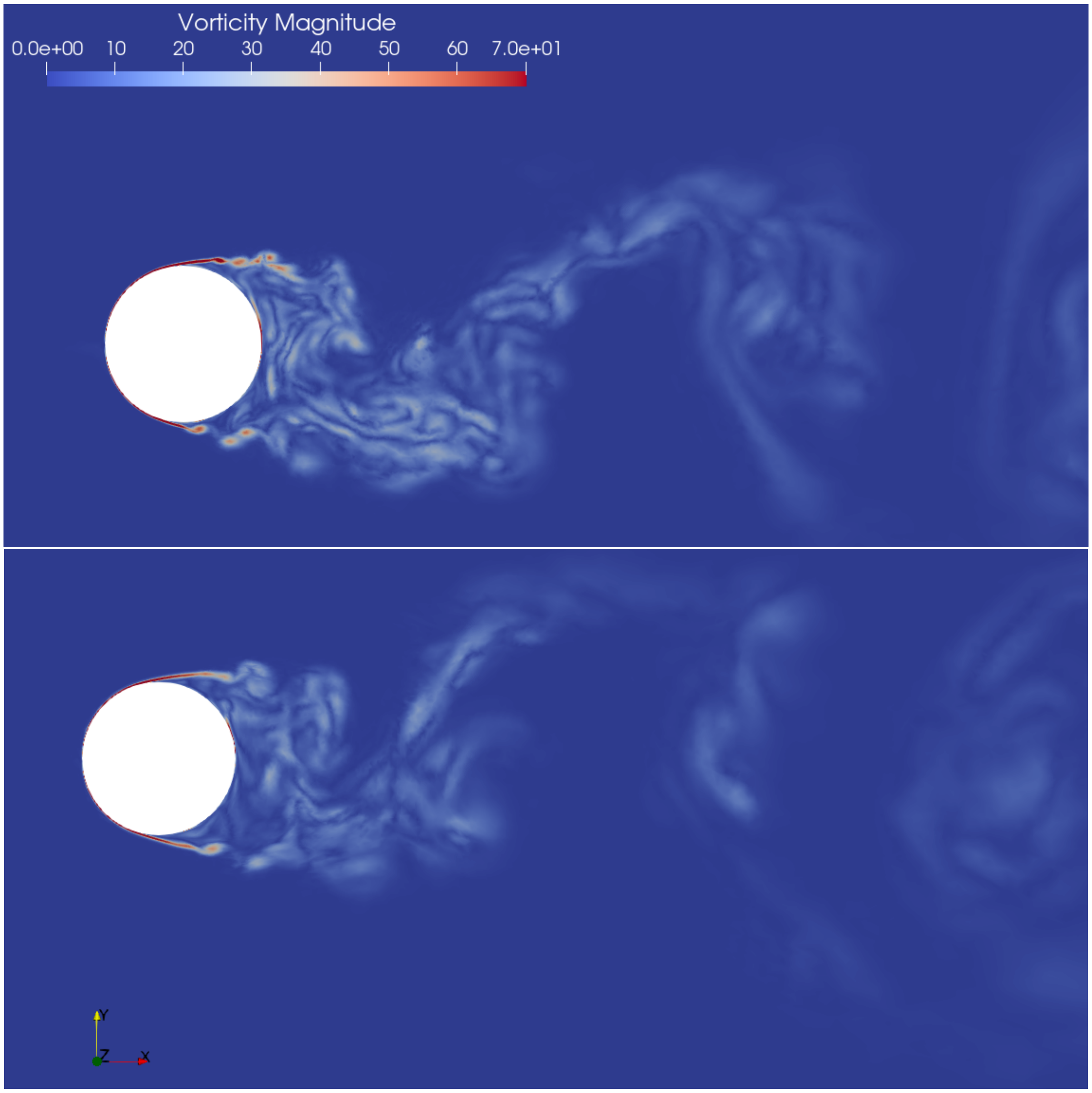

Figure 5: *Cylindre Re = 20K VMS-WALE results : Top, vorticity obtained with the new LES criterion, and bottom, vorticity obtained with Mach criterion only.*

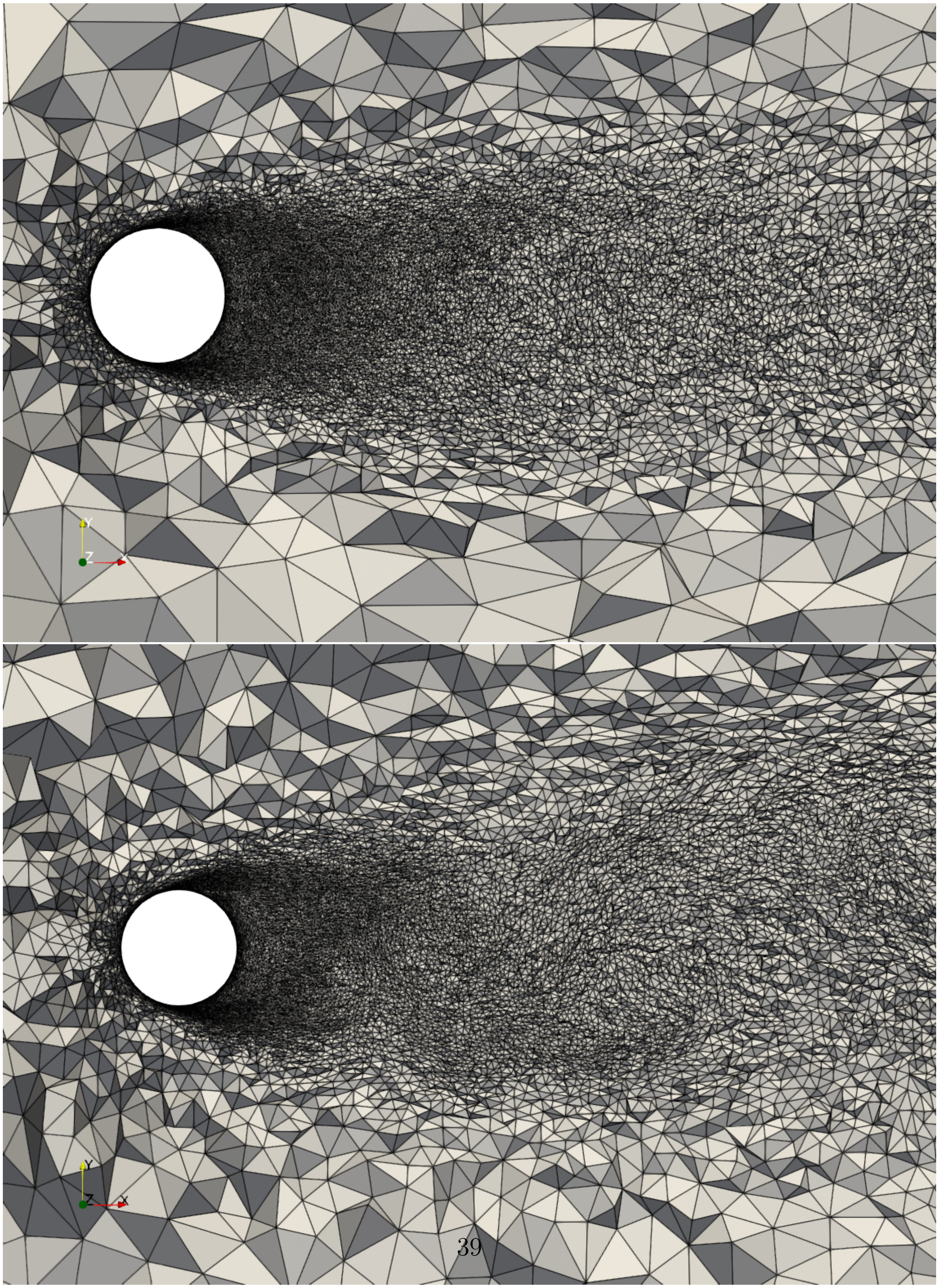

Figure 6: *Cylindre Re = 20K VMS-WALE results : Top, mesh obtained with the new LES criterion (around 1M vertices), and bottom, mesh obtained with Mach criterion only (around 1.1M vertices).*

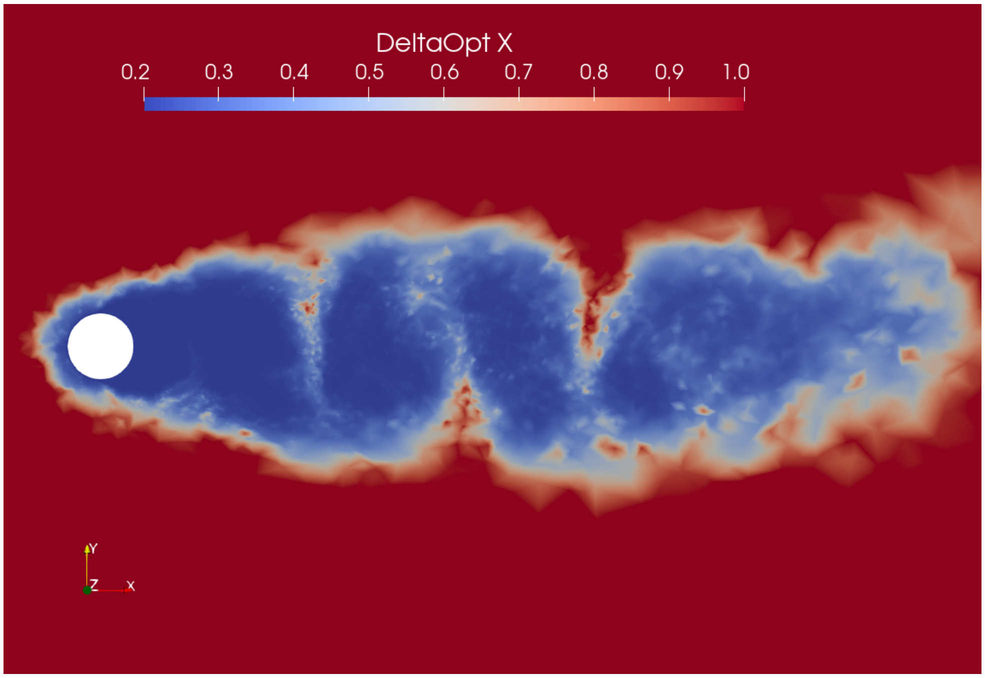

Figure 7: *Instantaneous value of* $\Delta_1^{opt}/\bar{\Delta}$ *for flow around a cylinder at* $Re = 20K$*. These values are those given by the algorithm with a choosen clamping.*

6.2 Mesh adaptive computation of a supercritical flow

At a Reynolds of 1M, the flow around the circular cylinder is supercritical, with a completely turbulent boundary layer. Computing with LES this boumdary layer is very expansive, and therefore such a strategy is not useful in industrial studies. However, this type of flow is frequently met in industry.

As options in NiceFlow, we start from the anisotropic mesh adaptation approach which was proven as very efficient for steady RANS flows, see for example [1],[11], and unsteady RANS, see [4].

For addressing both RANS regions and LES-type regions, we apply the DDES available in NiceFlow, defined initially in [**?**] also described in Chapter 3. This model is hybrid in the sense that in some "LES" regions, the model viscosity is very small, comparable to a SGS viscosity, while not being a Smagorinsky-like viscosity.

The rest of the algorithm which we apply is identical to the one applied to the two previous subcritical flows, with two stages of adaptation criteria: a Mach-Hessian criterion and its correction with the Toosi-Larsson analysis.

At this Reynolds number and with a limited number of vertices (around 1M), the DDES calculation produces a poorly fluctuating flow, although the model DDES viscosity is much lower in the wake than the RANS viscosity. We estimate that a more fluctuating solution would be obtained by running DDES with something like 3 times mode vertices. Our development was done on a lap top with 4 processors. A more ambitious calculation is starting but will take weeks.

However, the results are reasonable without the LES criterion and improved with the LES criterion.

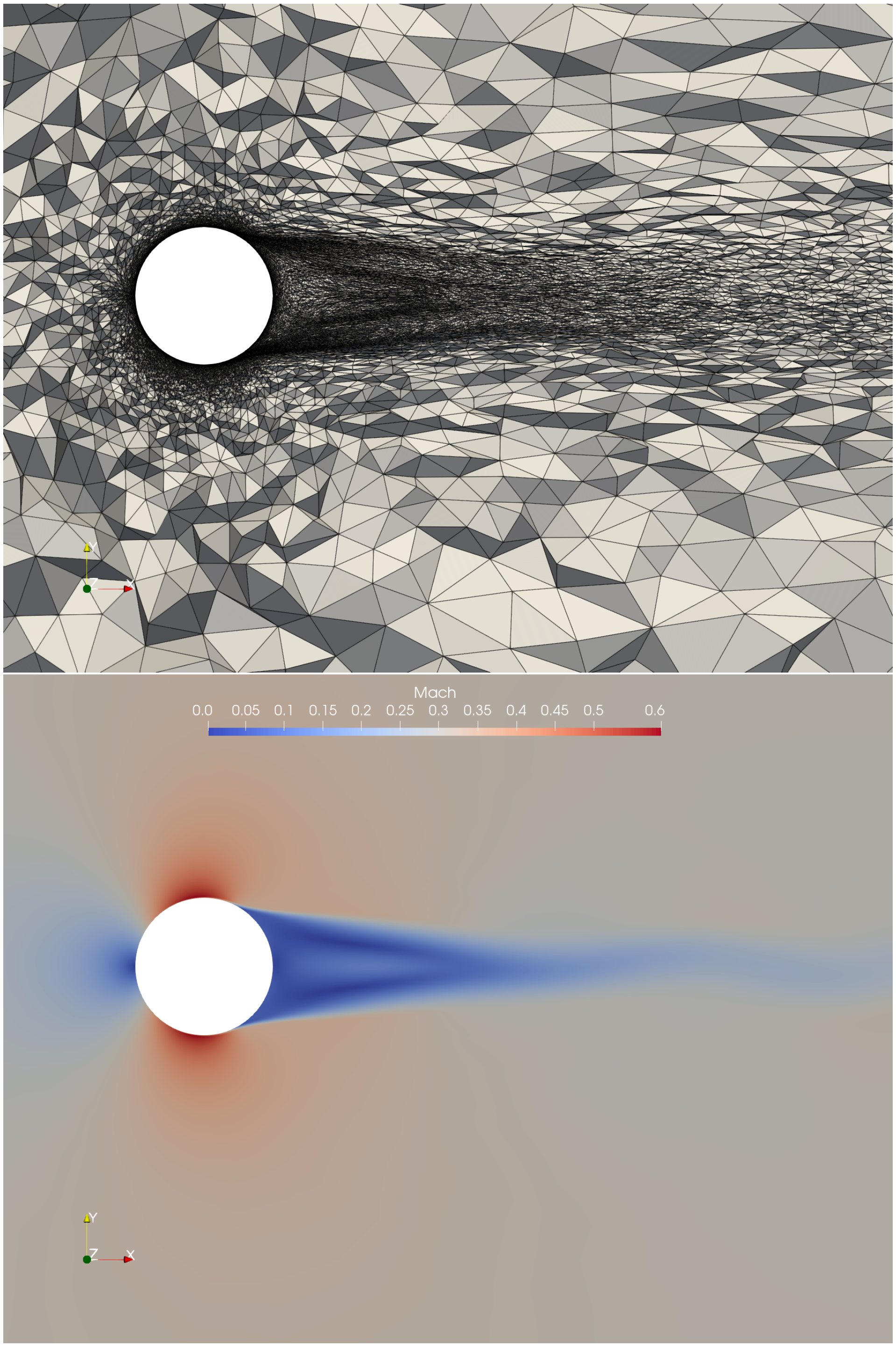

Figure 8: *Cylindre Re = 1M DDES results : Mesh (left) and Mach field (right) in cross-section for the new LES criterion. The mesh is around 1M vertices.*

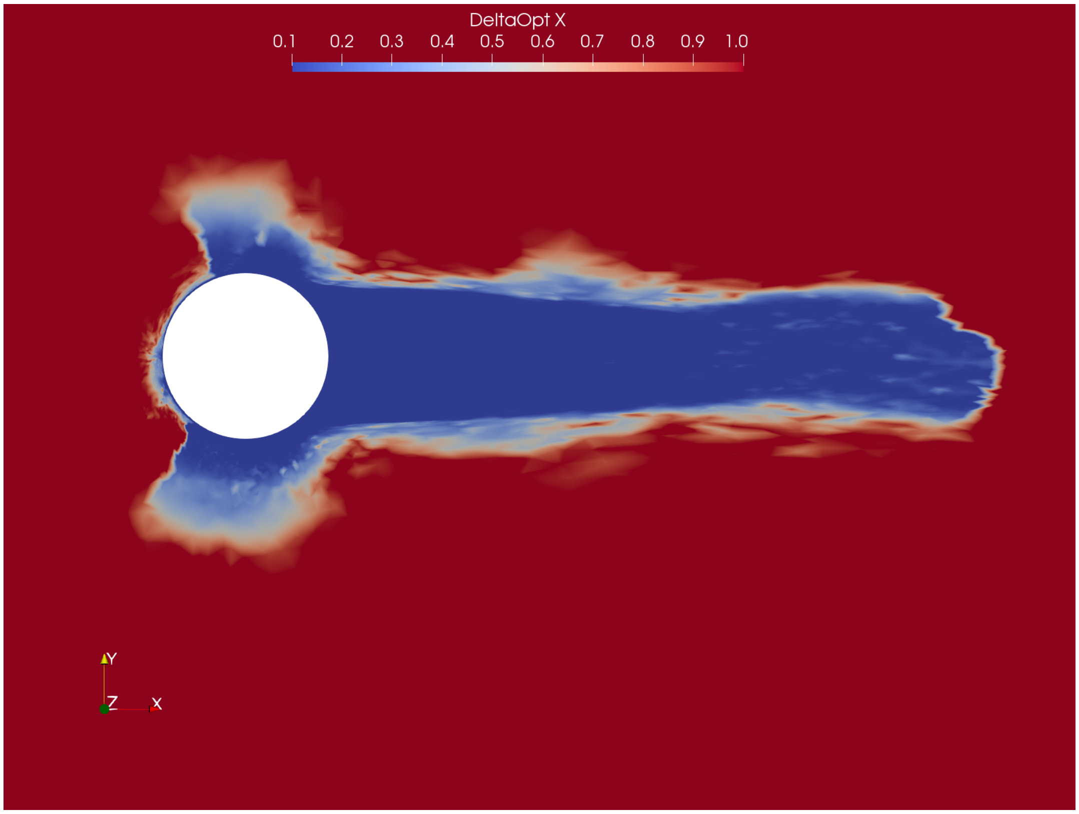

Figure 9: *Instantaneous value of* $\Delta_1^{opt}/\bar{\Delta}$ *for flow around a cylinder at* $Re = 1M$. *These values are those given by the algorithm with a choosen clamping.*

7 Concluding remarks

Anisotropic mesh adaptive CFD brings an important progress for applied numerical CFD. No more engineering time is spent for building meshes. Numerical results are mostly free of uncertainty concerning approximation errors. Our contribution aims at improving hybrid RANS/LES industrial calculations by proposing an anisotropic mesh adaptation.

To extend anisotropic mesh adaptation to the hybrid modelization, we propose a hybrid mesh adaptation. Indeed, LES error criteria are not able to refine many flow details like laminar boundary layers as well as RANS boundary layers. In contrast, the RANS-based mesh adaptation, in its feature-based or goal-oriented versions, contributes to a good global capture of the overall flow. For LES regions, we further adapt by extending the analysis of Toosi and Larsson which is based on the source term of LES-error equation. This second criterion is combined with the RANS criterion as a correcting factor for it. The combination is applied inside a transient fixed point adaptation algorithm with the option of using a single adapted mesh for the whole time interval.

Numerical examples concerning subcritical and supercritical vortex shedding flows past a circular cylinder. The subcritical cases uses a pure LES CFD model. The supercritical case applies our analysis to a DDES CFD model. Both experiences demonstrate the improvement brought by the proposed approach.

Of course these rather preliminar results should be completed by various other calculations before the efficiency of the new method is well delimited.

Several future methodological investigations can be identified.
- Our option of using a single mesh for the whole time interval (i.e. $kt_{max} = 1$) will be reconsidered and multiple mesh investigations will be undertaken in order to determinate in which conditions this second option is of interest.
- An important sequel of this developement would be to extend the analysis to the so-called goal-oriented analysis. In [10], the goal oriented analysis permitted to look for the best mesh for propagating an acoustic wave produced by an artificial acoustic source. With the new criterion, noise production by turbulence could be addressed.
- The introduction of the space-time adaptation as in [23] will be of interest in order to compute with optimally chosen time steps.

8 Acknowledgements

This work was supported by the ANR NORMA project, grant ANR-19-CE40-0020-01 of the French National Research Agency. The authors gratefully acknowledge GENCI for granted access to HPC resources through IDRIS (grant 2022-A0132A05067) and CINES (grants 2021-A0102A06386 and 2020-

A0092A05067).

References

[1] F. Alauzet and L. Frazza. 3D RANS anisotropic mesh adaptation on the high-lift version of NASA common research model (HL-CRM). *AIAA paper 2019-2947*, 2020.

[2] F. Alauzet and L. Frazza. Feature-based and goal-oriented anisotropic mesh adaptation for RANS applications in aeronautics and aerospace. *Journal of Computatiuonal Physics*, 439:110340, 2021.

[3] F. Alauzet, P.J. Frey, P.L. George, and B. Mohammadi. 3D transient fixed point mesh adaptation for time-dependent problems: Application to CFD simulations. *J. Comp. Phys.*, 222:592–623, 2007.

[4] F. Alauzet, A. Loseille, and G. Olivier. Time-accurate multi-scale anisotropic mesh adaptation for unsteady flows in CFD. *Journal of Computational Physics*, 373:28–63, 2018.

[5] F. Basile, J.-B. Chapelier, R. Laraufie, and P. Frey. hp-adaptive hybrid RANS/LES simulations for unstructured meshes with the discontinuous Galerkin method. *AIAA SCITECH 2022 Forum, Jan 2022, San Diego, United States. 10.2514/6.2022-1207. hal-03632119*, 2022.

[6] A. Belme, F. Alauzet, and A. Dervieux. A priori anisotropic goal-oriented estimate and mesh adaptation for viscous compressible flow. *Preprint*, 2017.

[7] A. Belme, A. Dervieux, and F. Alauzet. Time accurate anisotropic goal-oriented mesh adaptation for unsteady flows. *J. Comp. Phys.*, 231(19):6323–6348, 2012.

[8] M. Blind, A. Berk Kahraman, J. Larsson, and A. Beck. Grid-adaptation for wall-modeled Large Eddy Simulation using unstructured high-order methods. *arXiv:2301.03199v1*, 2023.

[9] S. Camarri, M.V. Salvetti, B. Koobus, and A. Dervieux. Large-eddy simulation of a bluff-body flow on unstructured grids. *Int. J. Num. Meth. Fluids*, 40:1431–1460, 2002.

[10] A. Carabias, A. Belme, A. Loseille, and A. Dervieux. Anisotropic goal-oriented error analysis for a third-order accurate CENO Euler discretization. *International Journal for Numerical Methods in Fluids*, 86(6):392–413, 2018.

[11] A. Dervieux, F. Alauzet, A. Loseille, and B. Koobus. *Mesh adaptation for Computational Fluid Dynamics, t.1 and t.2.* ISTE Ltd and John Wiley & Sons, 1st edition, 2023.

[12] G. Erlebacher, M. Y. Hussaini, C. G. Speziale, and T. A. Zang. Toward the large-eddy simulation of compressible turbulent flows. *Journal of Fluid Mechanics*, 238:155–185, 1992.

[13] K. J. Fidkowski. Output-based error estimation and mesh adaptation for unsteady turbulent flow simulations. *Computer Methods in Applied Mechanics and Engineering*, 2022.

[14] M. Germano, U. Piomelli, P. Moin, and W. Cabot. A dynamic subgrid-scale eddy viscosity model. *Phys. Fluids A*, 3(7):1760–1765, 1991.

[15] Sandip Ghosal. On the effect of numerical errors in large eddy simulations of turbulent flows. *Journal of Computational Physics*, 131:310–322, 1997.

[16] A. Hauser and G. Wittum. Adaptive Large Eddy Simulation. *Comput Visual Sei, 17:295-304 DOI 10.1007/s00791-016-0265-3*, 2015.

[17] Jeremy Ims and Z.J. Wang. A comparison of three error indicators for adaptive high-order Large Eddy Simulation. *Journal of Computational Physics*, 490:112312, 2023.

[18] A. G. Kravchenko and P. Moin. An analysis of numerical errors in Large-Eddy Simulations of turbulence. *Journal of Computational Physics*, 125:187–206, 1996.

[19] A. Loseille, A. Dervieux, and F. Alauzet. Fully anisotropic goal-oriented mesh adaptation for 3D steady Euler equations. *J. Comp. Phys.*, 229:2866–2897, 2010.

[20] C. Moussaed, S. Wornom, M.-V. Salvetti, B. Koobus, and A. Dervieux. Impact of Dynamic SubGrid-Scale modeling in Variational MultiScale

Large-Eddy Simulation of bluff-body flows. *Acta Mechanica*, 225:3309–3323, 2014.

[21] F. Naddei. Simulation adaptative des grandes échelles d'écoulements turbulents fondée sur une méthode Galerkine discontinue. *Numerical Analysis [cs.NA]. Université Paris Saclay (COmUE), 2019. English. NNT : 2019SACLX060*, 2019.

[22] D. Papadogiannis, L. Billon, and F. Alauzet. Isotropic and anisotropic mesh adaptation for RANS simulations of a nacelle under crosswind conditions. *Proceedings of Global Power and Propulsion Society, GPPS Chania22, september 12-14, 2022. www.gpps.global,ISSN-Nr: 2504-4400*, 2022.

[23] B. Sauvage, F. Alauzet, and A.Dervieux. A space and time fixed point mesh adaptation method. *Accepted for publication in J. Comp. Phys.*, 2024.

[24] B. Sauvage, F. Alauzet, and A. Dervieux. A space and time fixed point adaptation method. Deliverable T4-D3, ANR Norma, 2022.

[25] J. Smagorinsky. General circulation experiments with the primitive equations. *Monthly Weather Review*, 91(3):99–164, 1963.

[26] P. R. Spalart, S. Deck, M. L. Shur, K. D. Squires, M. Kh. Strelets, and A. K. Travin. A new version of detached-eddy simulation, resistant to ambiguous grid densitie. *Theoritical and Computational Fluid Dynamic*, 20(3):181–195, 2006.

[27] P.R. Spalart and S.R. Allmaras. A one-equation turbulence model for aerodynamic flows. In *30th AIAA Aerospace Sciences Meeting and Exhibit*, AIAA-92-0439, Reno, NV, USA, Jan 1992.

[28] S. Toosi and J. Larsson. Towards systematic grid selection in LES: identifying the optimal spatial resolution by minimizing the solution sensitivity. *Computers and Fluids, doi:https://doi.org/10.1016/j.compfluid.2020.*, 201:104488, 2020.

[29] S. Toosi and J. Larsson. The Germano identity error and the residual of the LES governing equation. *Journal of Computational Physics*, 443:110544, 2021.